



US009757092B2

(12) **United States Patent**
Oraevsky et al.

(10) **Patent No.:** **US 9,757,092 B2**
(45) **Date of Patent:** **Sep. 12, 2017**

(54) **METHOD FOR DUAL MODALITY OPTOACOUSTIC IMAGING**

(58) **Field of Classification Search**
CPC A61B 5/0095
(Continued)

(71) Applicant: **Seno Medical Instruments, Inc.**, San Antonio, TX (US)

(56) **References Cited**

(72) Inventors: **Alexander A. Oraevsky**, Houston, TX (US); **Sergey A. Ermilov**, Houston, TX (US); **Andre Conjusteau**, Houston, TX (US); **Peter Brecht**, Santa Monica, CA (US); **Vyacheslav Nadvoretzkiy**, Houston, TX (US); **Richard Su**, Sugar Land, TX (US); **Donald G. Herzog**, Collingswood, NJ (US); **Bryan Clingman**, Chandler, AZ (US); **Jason Zalev**, Thornhill (CA)

U.S. PATENT DOCUMENTS

4,651,850 A 3/1987 Matsuo
5,293,873 A 3/1994 Fang
(Continued)

FOREIGN PATENT DOCUMENTS

EP 0282234 A1 9/1988
EP 1493380 A1 1/2005
(Continued)

(73) Assignee: **Seno Medical Instruments, Inc.**, San Antonio, TX (US)

OTHER PUBLICATIONS

(*) Notice: Subject to any disclaimer, the term of this patent is extended or adjusted under 35 U.S.C. 154(b) by 515 days.

Holan, Scott H., and John A. Viator. "Automated wavelet denoising of photoacoustic signals for circulating melanoma cell detection and burn image reconstruction." *Physics in medicine and biology* 53.12 (2008): N227.*

(Continued)

(21) Appl. No.: **13/667,830**

Primary Examiner — Andrew Moyer

(22) Filed: **Nov. 2, 2012**

(74) *Attorney, Agent, or Firm* — Harness, Dickey & Pierce, P.L.C.

(65) **Prior Publication Data**

US 2013/0301380 A1 Nov. 14, 2013

Related U.S. Application Data

(63) Continuation-in-part of application No. 13/507,217, filed on Jun. 13, 2012, now Pat. No. 9,289,191, which
(Continued)

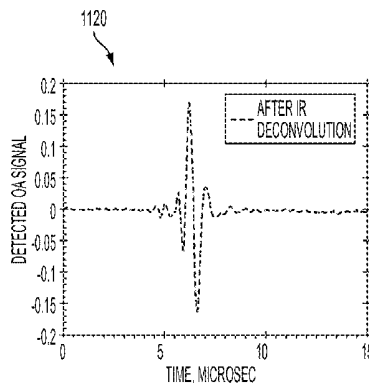
(57) **ABSTRACT**

A real-time imaging method that provides ultrasonic imaging and optoacoustic imaging coregistered through application of the same hand-held probe to generate and detect ultrasonic and optoacoustic signals. These signals are digitized, processed and used to reconstruct anatomical maps superimposed with maps of two functional parameters of blood hemoglobin index and blood oxygenation index. The blood hemoglobin index represents blood hemoglobin concentration changes in the areas of diagnostic interest relative to the background blood concentration. The blood oxygenation index represents blood oxygenation changes in the areas of diagnostic interest relative to the background level of blood oxygenation. These coregistered maps can be used

(Continued)

(51) **Int. Cl.**
G06K 9/00 (2006.01)
A61B 8/08 (2006.01)
(Continued)

(52) **U.S. Cl.**
CPC **A61B 8/5215** (2013.01); **A61B 5/0035** (2013.01); **A61B 5/0095** (2013.01);
(Continued)



to noninvasively differentiate malignant tumors from benign lumps and cysts.

15 Claims, 28 Drawing Sheets

Related U.S. Application Data

is a continuation-in-part of application No. 13/341,950, filed on Dec. 31, 2011, now Pat. No. 8,686,335, which is a continuation-in-part of application No. 13/287,759, filed on Nov. 2, 2011.

- (51) **Int. Cl.**
A61B 5/00 (2006.01)
A61B 8/00 (2006.01)
- (52) **U.S. Cl.**
 CPC *A61B 8/4416* (2013.01); *A61B 8/48* (2013.01); *A61B 8/5207* (2013.01); *A61B 8/5261* (2013.01); *A61B 8/4477* (2013.01); *A61B 8/4494* (2013.01); *A61B 8/481* (2013.01)
- (58) **Field of Classification Search**
 USPC 382/128
 See application file for complete search history.

(56) **References Cited**

U.S. PATENT DOCUMENTS

5,341,204 A 8/1994 Grant et al.
 5,348,002 A 9/1994 Caro
 5,460,182 A 10/1995 Goodman et al.
 5,504,281 A 4/1996 Whitney et al.
 5,830,146 A 11/1998 Skladnev et al.
 5,840,023 A 11/1998 Oraevsky et al.
 5,935,288 A 8/1999 DiGiovanni et al.
 5,977,538 A 11/1999 Unger et al.
 6,216,025 B1 4/2001 Kruger
 6,263,094 B1 7/2001 Rosich et al.
 6,617,559 B1 9/2003 Emery et al.
 6,979,292 B2 12/2005 Kanayama et al.
 7,675,013 B2 3/2010 Kobayashi et al.
 7,741,900 B1 6/2010 Li
 8,109,981 B2 2/2012 Gertner et al.
 8,327,973 B2 12/2012 Parish et al.
 8,480,584 B2 7/2013 Kanayama et al.
 8,686,335 B2 4/2014 Schmid et al.
 9,226,666 B2 1/2016 Wang et al.
 9,289,191 B2 3/2016 Clingman et al.
 2003/0139672 A1 7/2003 Cane et al.
 2004/0167619 A1 8/2004 Case et al.
 2005/0004458 A1 1/2005 Kanayama et al.
 2005/0070801 A1 3/2005 Yamashita et al.
 2005/0105877 A1 5/2005 Nappi et al.
 2005/0187471 A1* 8/2005 Kanayama et al. 600/437
 2005/0261568 A1 11/2005 Hular et al.
 2006/0167531 A1 7/2006 Gertner et al.
 2007/0081711 A1* 4/2007 Kim et al. 382/128
 2007/0093702 A1 4/2007 Yu et al.
 2007/0238958 A1 10/2007 Oraevsky et al.
 2008/0051655 A1 2/2008 Sato et al.
 2008/0071172 A1 3/2008 Bruck et al.
 2008/0172111 A1* 7/2008 Anderson et al. 607/89
 2008/0177183 A1 7/2008 Courtney et al.
 2008/0255433 A1 10/2008 Prough et al.
 2009/0000383 A1 1/2009 Knowles et al.
 2009/0124902 A1 5/2009 Herrmann
 2009/0149761 A1* 6/2009 Zou et al. 600/476
 2009/0156932 A1 6/2009 Zharov
 2009/0187099 A1 7/2009 Burcher
 2009/0263001 A1 10/2009 Ding et al.
 2010/0049044 A1* 2/2010 Burcher A61B 5/0059
 600/437

2010/0053618 A1 3/2010 Nakajima et al.
 2010/0056916 A1* 3/2010 Bakker et al. 600/443
 2010/0094134 A1 4/2010 Zhu et al.
 2010/0154547 A1 6/2010 Fukada et al.
 2010/0174190 A1 7/2010 Hancock et al.
 2010/0249570 A1 9/2010 Carson et al.
 2010/0256496 A1 10/2010 Zhu
 2010/0285518 A1 11/2010 Viator et al.
 2011/0054292 A1 3/2011 Hirson et al.
 2011/0088477 A1 4/2011 Someda et al.
 2011/0091423 A1 4/2011 Kempf et al.
 2011/0098572 A1 4/2011 Chen et al.
 2011/0106478 A1 5/2011 Someda
 2011/0118606 A1 5/2011 Kim
 2011/0178401 A1 7/2011 Ichihara et al.
 2011/0201914 A1* 8/2011 Wang A61B 5/0059
 600/407
 2011/0231160 A1* 9/2011 Suzuki 702/189
 2011/0303015 A1 12/2011 Ichihara et al.
 2011/0319743 A1 12/2011 Satoh
 2012/0289812 A1 11/2012 Oishi
 2013/0039147 A1 2/2013 Witte et al.
 2013/0041267 A1 2/2013 Ntziachristos et al.
 2013/0060140 A1 3/2013 Sinelnikov
 2013/0064771 A1 3/2013 Wada
 2013/0109950 A1 5/2013 Herzog et al.
 2013/0112001 A1 5/2013 Furukawa
 2013/0190591 A1 7/2013 Hirson et al.
 2013/0190595 A1 7/2013 Oraevsky et al.
 2013/0310688 A1 11/2013 Rosen et al.
 2014/0194723 A1 7/2014 Herzog et al.

FOREIGN PATENT DOCUMENTS

JP 2008049063 A 3/2008
 JP 2010125260 A 6/2010
 JP 2013-202050 A 10/2013
 JP 2013-255707 A 12/2013
 WO 0110295 A1 2/2001
 WO 2004010866 A1 2/2004
 WO 2006061829 A1 6/2006
 WO 2011091423 7/2011
 WO 2011098101 A1 8/2011
 WO 2011137385 A1 11/2011

OTHER PUBLICATIONS

Lu, Tao, and Huiyong Mao. "Deconvolution algorithm with LTI Wiener filter in photoacoustic tomography." 2009 Symposium on Photonics and Optoelectronics. IEEE, 2009.*
 Kossoff, George, Elizabeth Kelly Fry, and Jack Jellins. "Average velocity of ultrasound in the human female breast." The Journal of the Acoustical Society of America 53.6 (1973): 1730-1736.*
 ISA/KR, International Search Report, Int'l Application No. PCT/US12/63409, Mar. 25, 2013, p. 4.
 J.J. Niederhauser, M. Jaeger, M. Frenz: Comparison of laser-induced and classical ultrasound. Proc. SPIE Jan. 2003, v. 4960, 118-123.
 S.Y. Emelianov, S.R. Aglyamov, J. Shah, S. Sethuraman, W.G. Scott, R. Schmitt, M. Motamedi, A. Karpouk, A.A. Oraevsky: Combined ultrasound, optoacoustic and elasticity imaging, Proc. SPIE Jan. 2004, v. 5320: 101-112.
 J. J. Niederhauser, M. Jaeger, R. Lemor, P. Weber and M. Frenz, "Combined ultrasound and optoacoustic system for real-time high-contrast vascular imaging in vivo," IEEE Trans Med Imaging v 24(4), 436-440 (2005).
 S. Ermilov, M. Fronheiser, H.-P. Brecht, R. Su, A. Conjusteau, K. Mehta, P. Otto, A. Oraevsky: Development of laser optoacoustic and ultrasonic imaging system for breast cancer utilizing handheld array probes; Proc. SPIE vol. 7177: 717703, pp. 1-10 (2009).
 A.A. Oraevsky, S.L. Jacques, F.K. Tittel: Determination of tissue optical properties by piezoelectric detection of laser-induced stress waves; Proc. SPIE vol. 1882 (1993).
 A.A. Oraevsky, S.L. Jacques, R.O. Esenaliev, and F.K. Tittel: Time-Resolved Optoacoustic Imaging in Layered Biological Tis-

(56)

References Cited

OTHER PUBLICATIONS

sues; OSA Proceedings on Advances in Optical Imaging and Photon Migration, 1994, vol. 21, pp. 161-165.

R.O. Esenaliev, A.A. Oraevsky, S.L. Jacques, and F.K. Tittel: Laser opto-acoustic tomography for medical diagnostics: Experiments with biological tissues; SPIE vol. 2676, pp. 84-90 (1996).

A. Karabutov, V. Letokhov, and N. Podymova: Time-resolved opto-acoustic tomography of inhomogeneous media; SPIE vol. 2389, pp. 209-217 (1995).

A.A. Oraevsky, S.L. Jacques, R.O. Esenaliev, F.K. Tittel: Direct measurement of laser fluence distribution and optoacoustic imaging in heterogeneous tissues; SPIE vol. 2323, pp. 37-46 (1995).

A.A. Oraevsky, R.O. Esenaliev, S.L. Jacques, and F.K. Tittel: Laser opto-acoustic tomography for medical diagnostics: principles; SPIE vol. 2676, pp. 22-31 (1996).

A.A. Oraevsky, R. Esensaliev, S.L. Jacques, S. Thomsen, and F.K. Tittel: Lateral and z-axial resolution in laser optoacoustic imaging with ultrasonic transducers; SPIE vol. 2389, pp. 198-208.

"MatLab: Programming Fundamentals", The Math Works, Inc., R2011 b, 2011.

Aziz et al. 2011 Optik 122:1462-1465.

Castelino, Robin; "Biomedical Applications of Photoacoustics for Thermal Therapy", 2008.

Dahl, Jeremy J. and Trahey, Gregg E., "Off-Axis Scatterer Filters for Improved Aberration Measurements", 2003 IEEE Ultrasonics Symposium- 344, 2003.

Fronheiser et al. 2010 J. Biomed. Optics 15:021305-1—021305-7.

Intel, Intel Integrated Performance Primitives for Intel Architecture, Reference Manual, vol. 2: Image and Video Processing, Sep. 2007.

Jiang, Zhen, et al. "Different optical spectral characteristics in a necrotic transmissible venereal tumor and a cystic lesion in the same canine prostate observed by triple-band trans-rectal optical tomography under trans-rectal ultrasound guidance." SPIE BIOS. International Society for Optics and Photonics, 2011.

Kingsbury, "Complex Wavelets for Shift Invariant Analysis and Filtering of Signals", Journal of Applied and computational Harmonic Analysis, vol. 10, No. 3, May 2001, pp. 234-253.

Kuchment, P. et al., "Mathematics of Photoacoustic and Thermoacoustic Tomography", Mathematics Dept., Texas A&M University, Dec. 10, 2009.

Ma, Rui, et al. "Multispectral optoacoustic tomography (MSOT) scanner for whole-body small animal imaging." Optics express 17.24 (2009): 21414-21426.

Misiti, Michel et al., "Wavelet Toolbox", The MathWorks, Inc., User's Guide, Version 1, 1996.

Munch, Beat et al., "Stripe and ring artifact removal with combined wavelet— Fourier filtering", Optics Express 8567, vol. 17, No. 10, May 11, 2009.

Nguyen, "A Family of Inversion Formulas in Thermoacoustic Tomography", Department of Mathematics, Texas A&M University, Mar. 5, 2009.

O'Donnell, Matthew et al., "Correlation-Based Aberration Correction in the Presence of Inoperable Elements", IEEE Transactions of Ultrasonics, Ferroelectrics, and Frequency Control, vol. 39, No. 6, Nov. 1992.

Otto et al., "Coregistration of Angiogenesis Related Hemoglobin and Tissue Density in breast tumors using opto-acoustic imaging combined with ultrasound", 2009.

Sendur et al., "Bivariate Shrinkage Functions for Wavelet-Based Denoising Exploiting Interscale Dependency", IEEE Transactions on Signal Processing, vol. 50, No. 11, Nov. 2002.

Wang, Yi, et al. "Photoacoustic imaging with deconvolution algorithm." Physics in medicine and biology 49.14 (2004): 3117.

Wang, Yu, et al. "Integrated photoacoustic and fluorescence confocal microscopy." IEEE Transactions on Biomedical Engineering 57.10 (2010): 2576-2578.

Zhu, Qing, Susan Tannenbaum, and Scott H. Kurtzman. "Optical tomography with ultrasound localization for breast cancer diagnosis and treatment monitoring." Surgical oncology clinics of North America 16.2 (2007): 307-321.

* cited by examiner

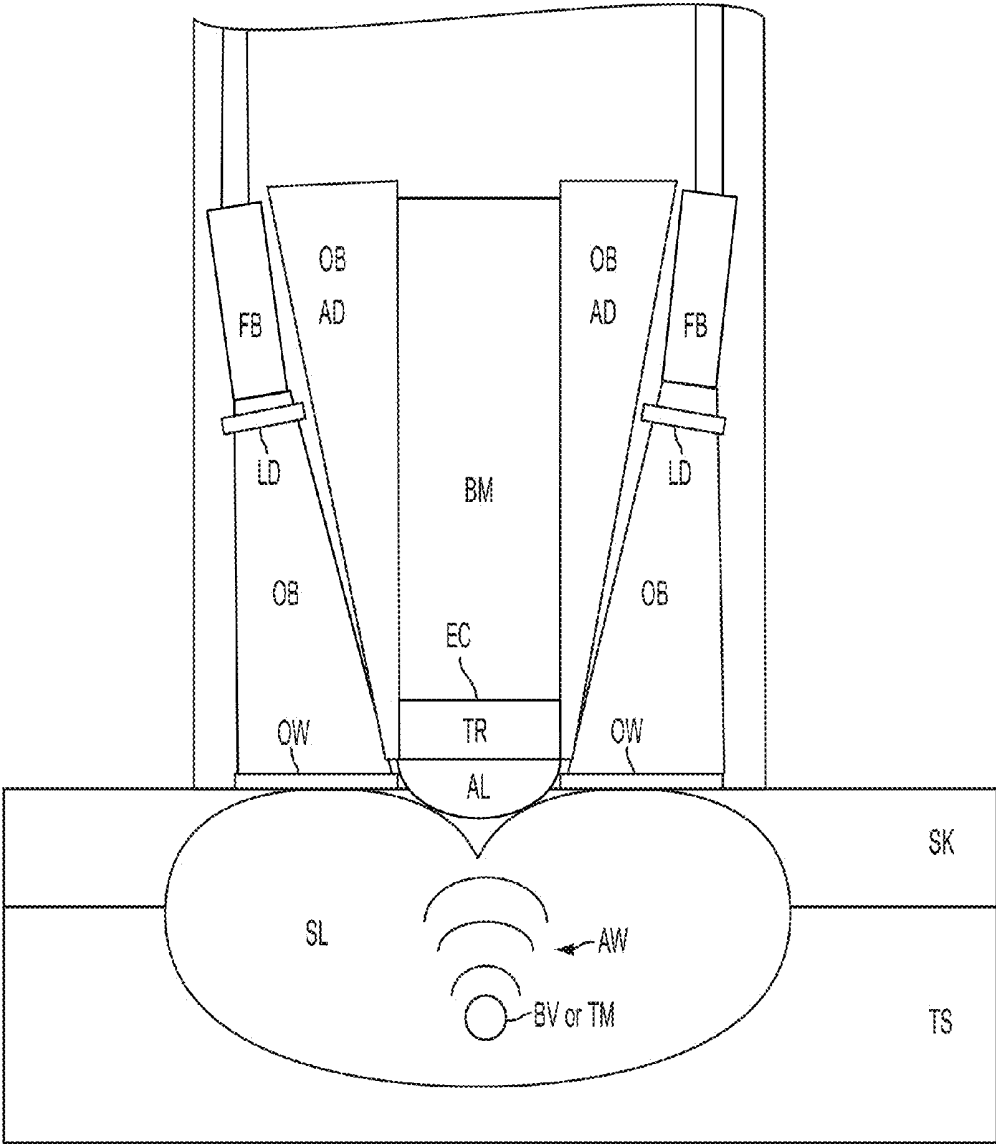


FIG. 1A

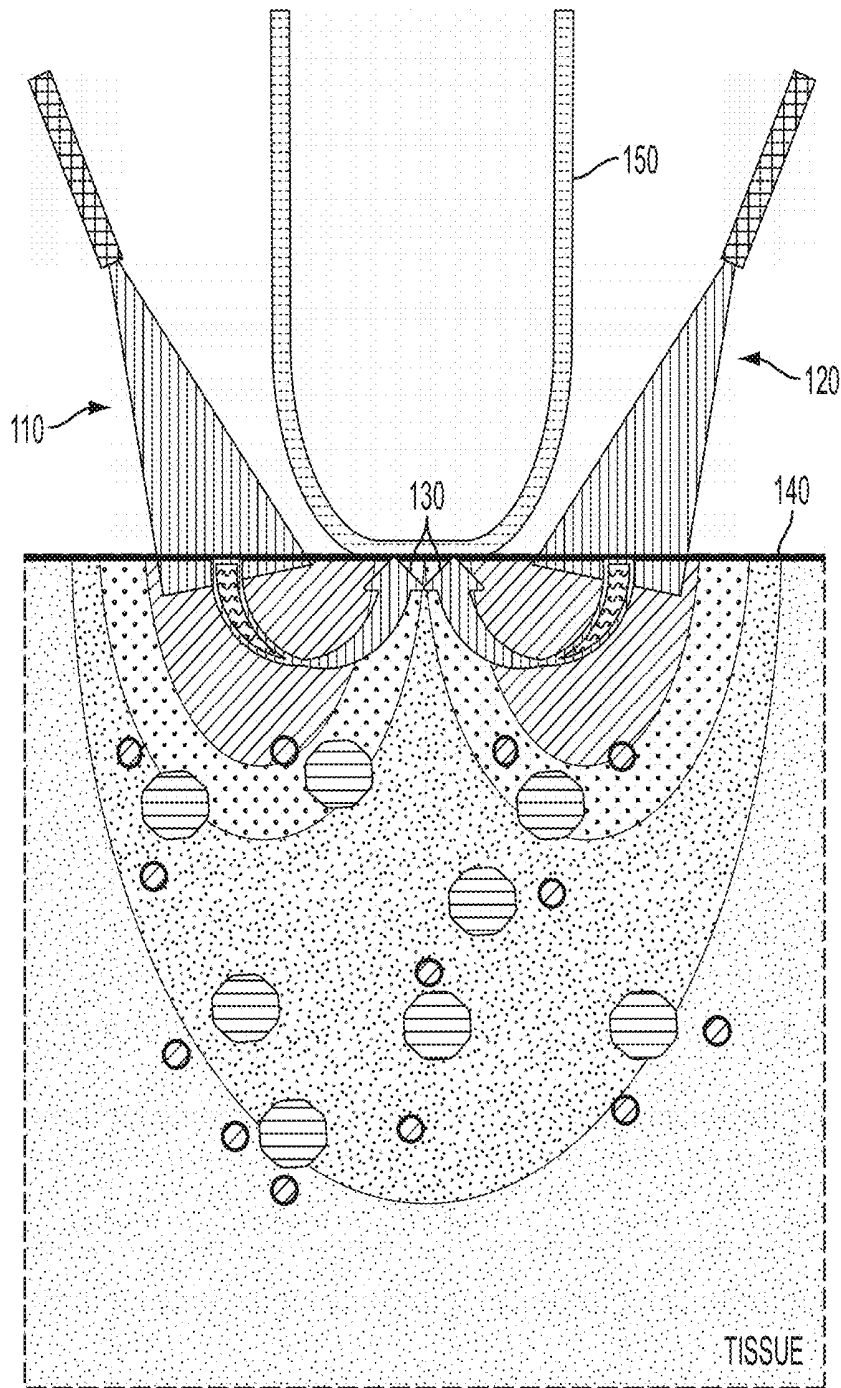


FIG. 1B

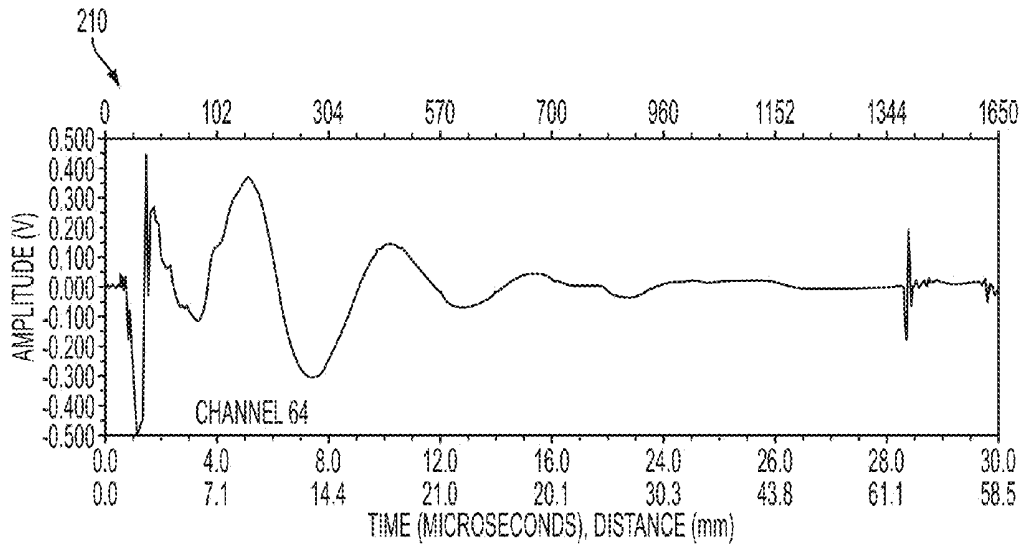


FIG. 2A

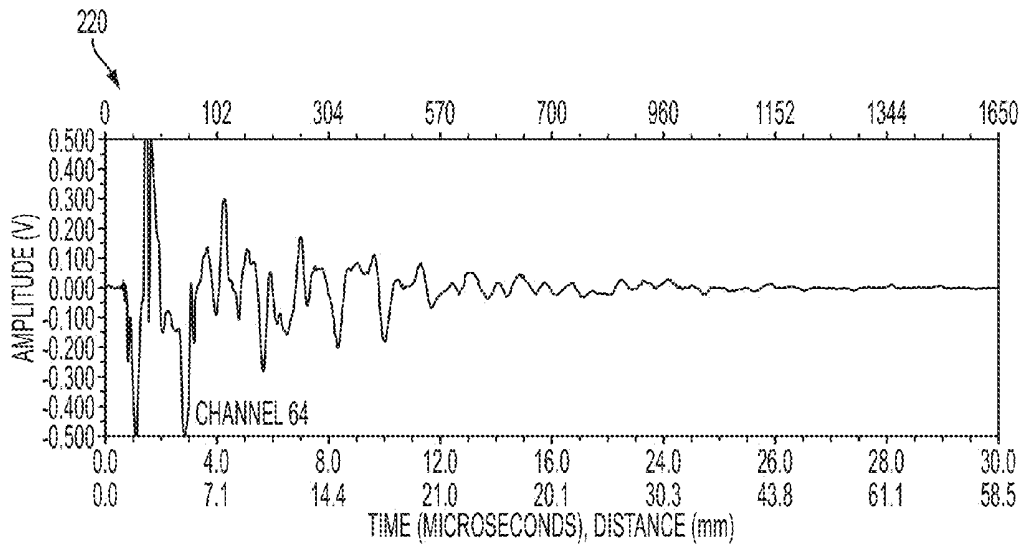


FIG. 2B

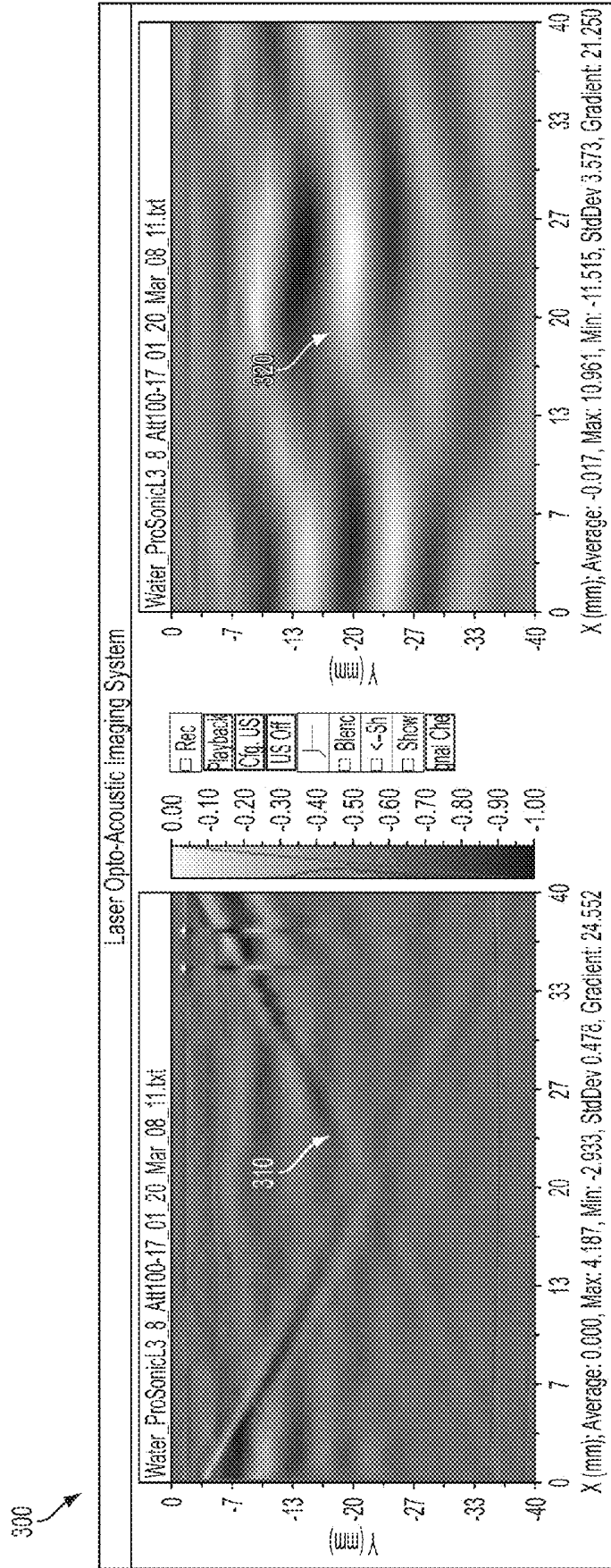


FIG. 3

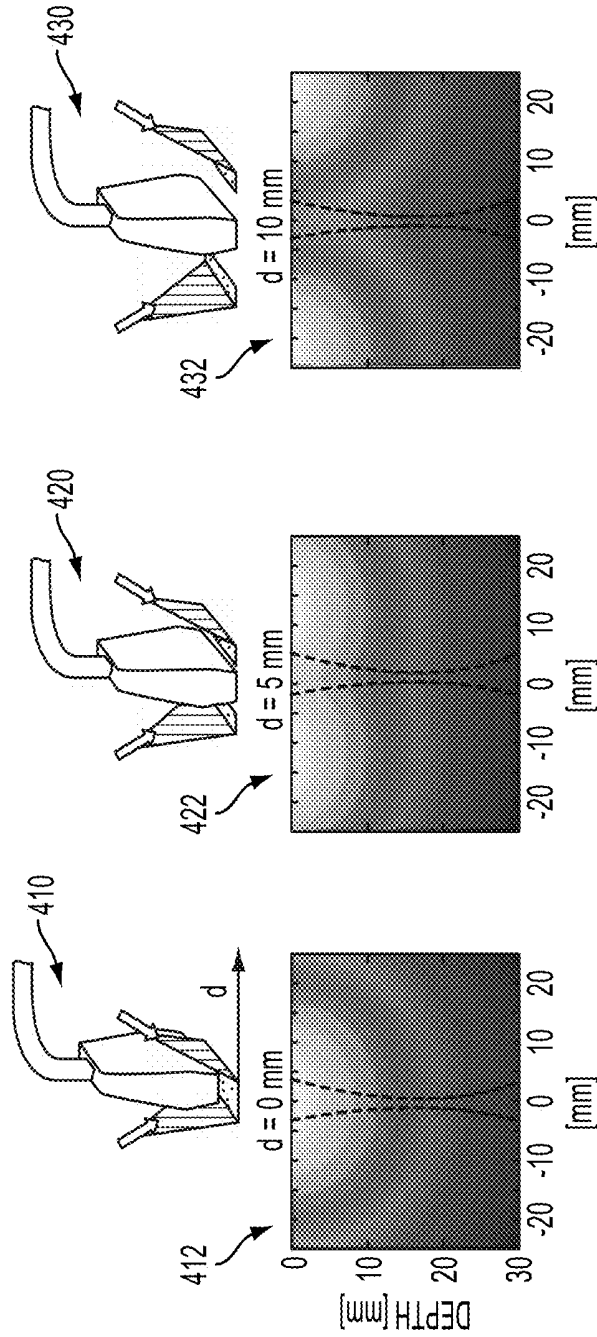


FIG. 4C

FIG. 4B

FIG. 4A

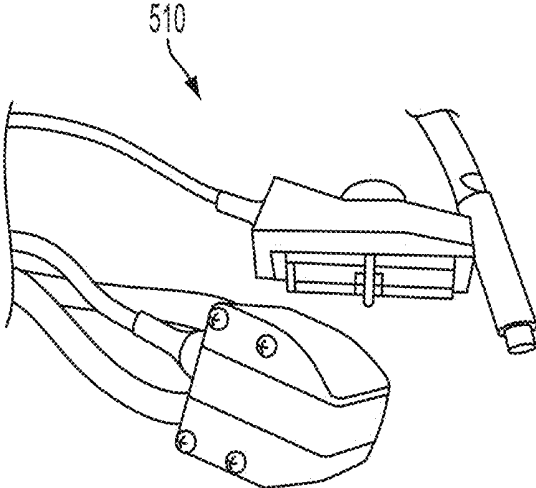


FIG. 5A

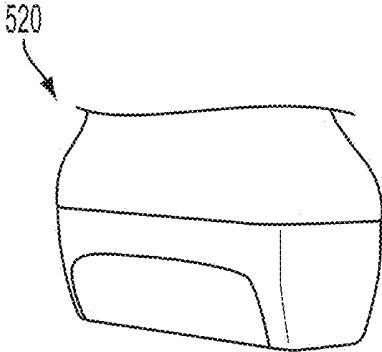


FIG. 5B

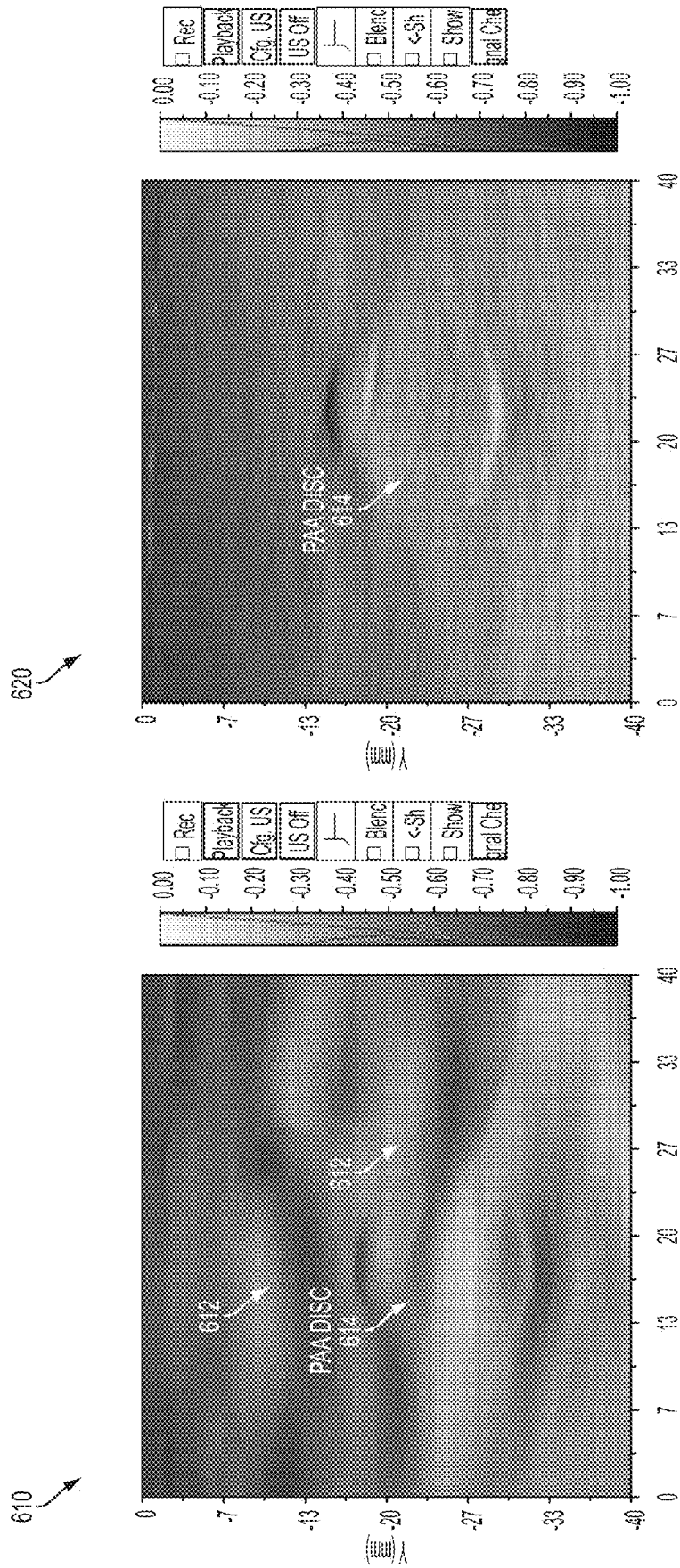


FIG. 6

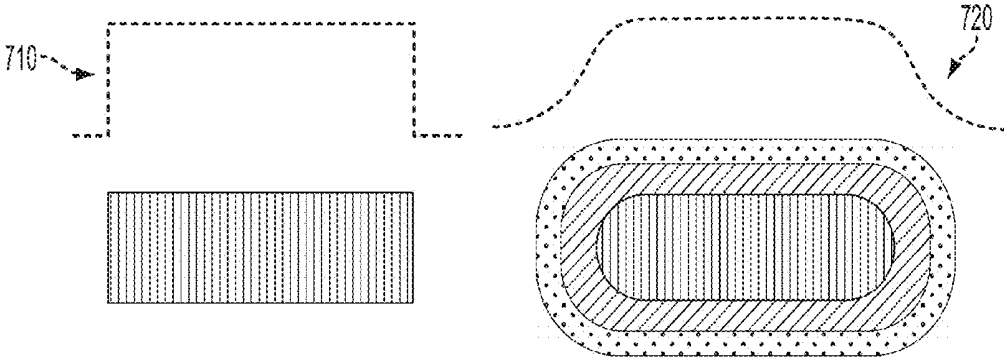


FIG. 7A



FIG. 7B

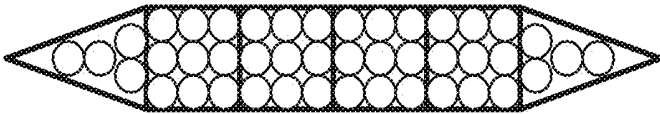


FIG. 7C

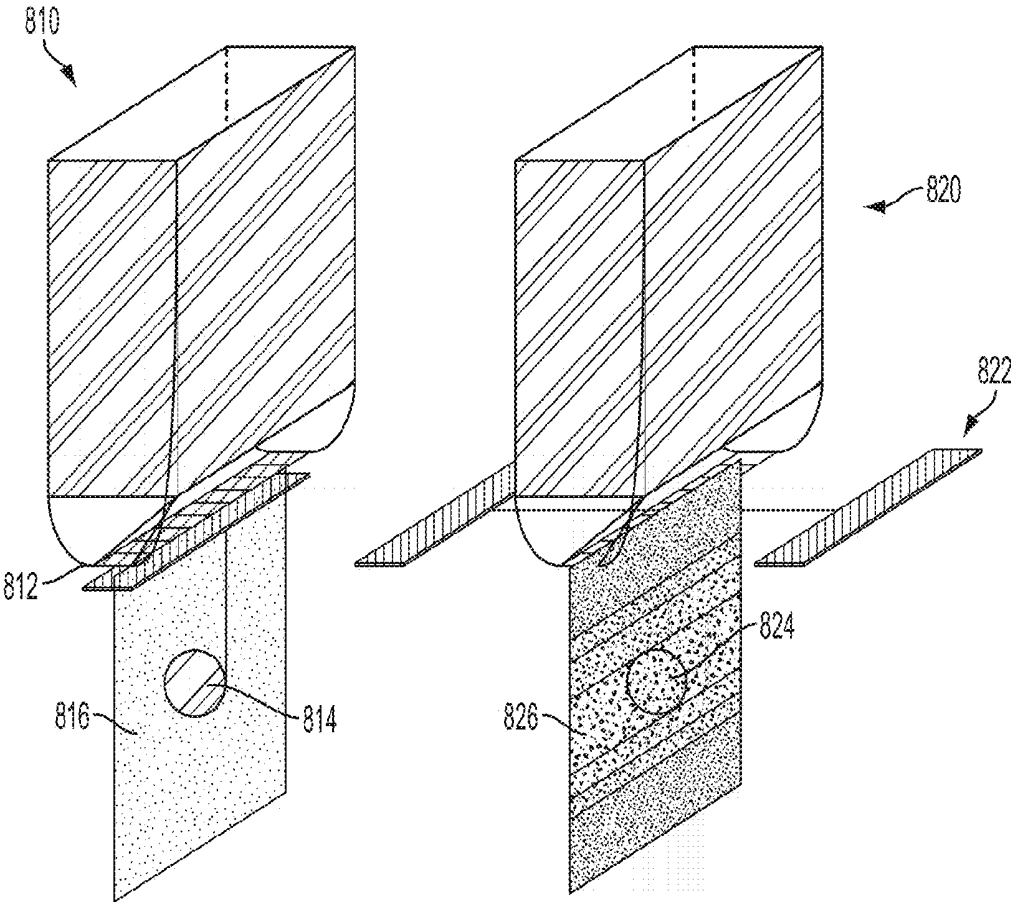


FIG. 8

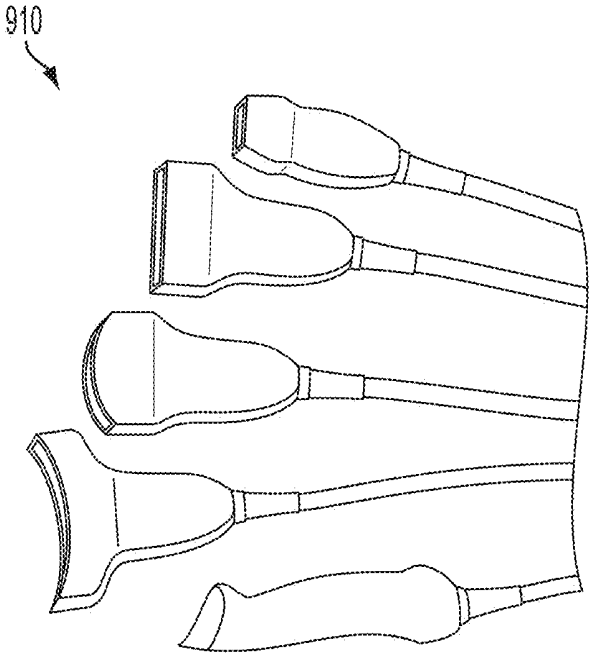


FIG. 9A

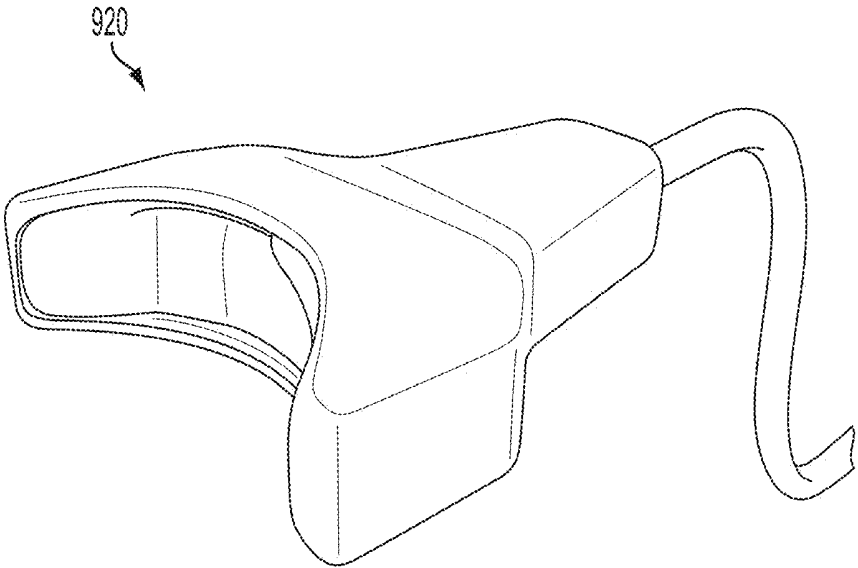


FIG. 9B

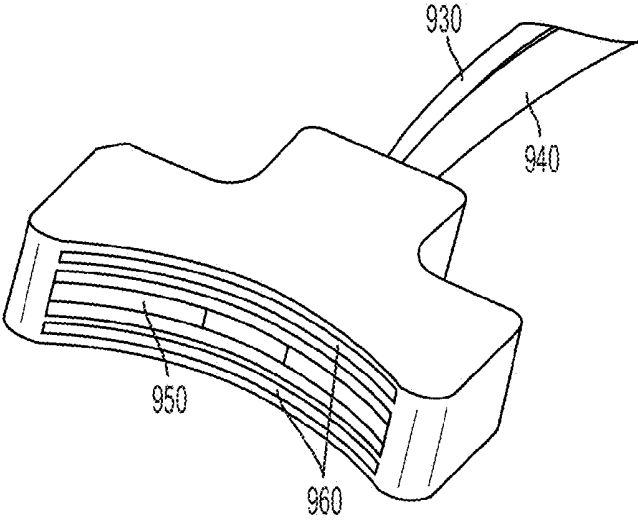


FIG. 9C

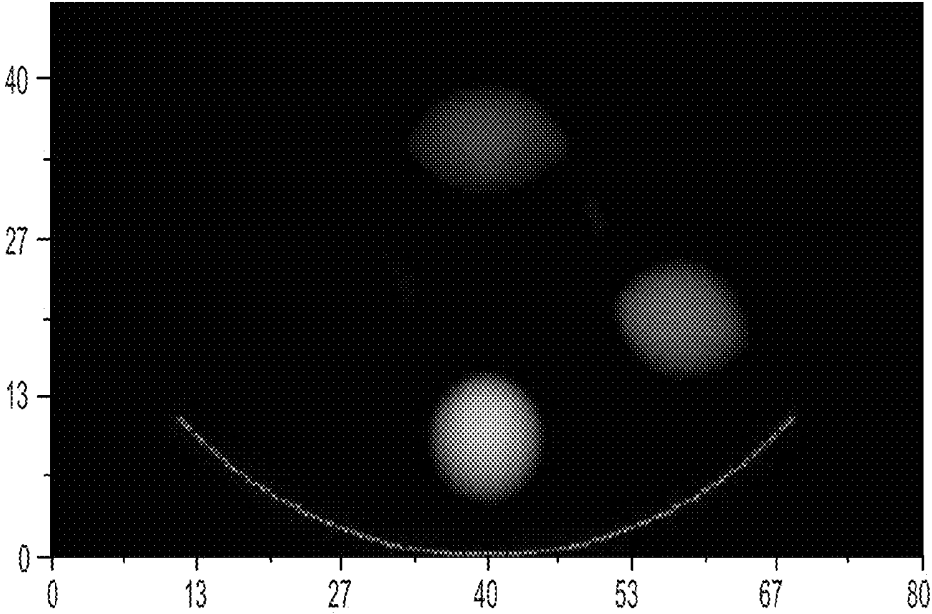


FIG. 9D

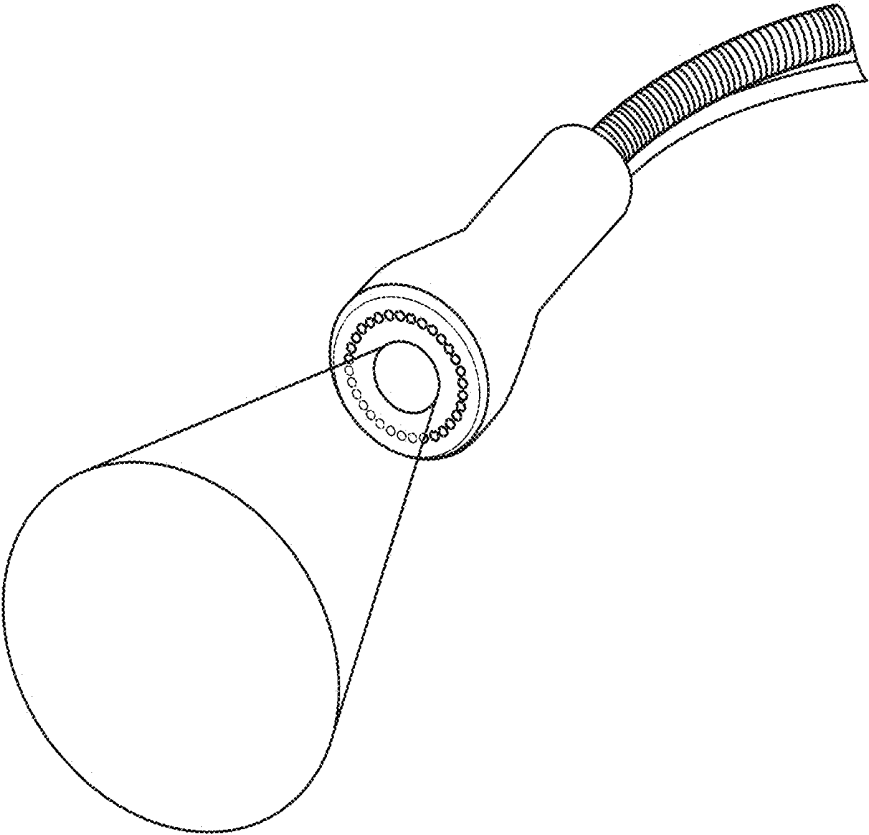


FIG. 9E

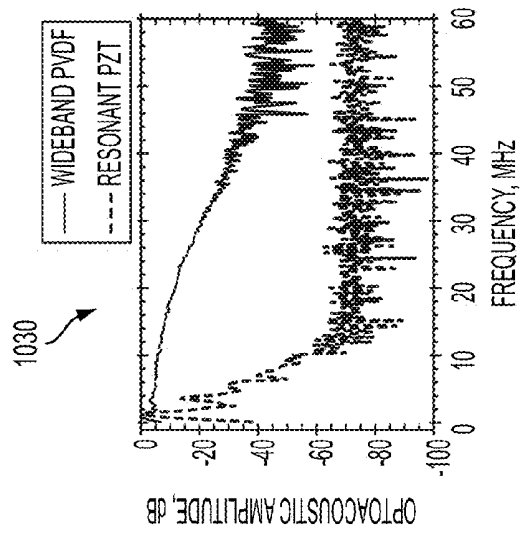


FIG. 10C

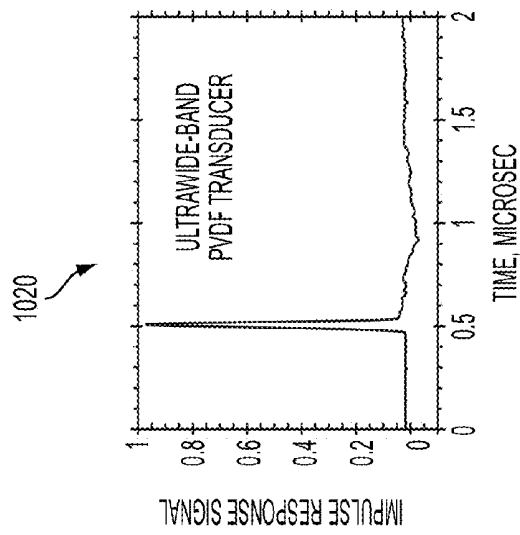


FIG. 10B

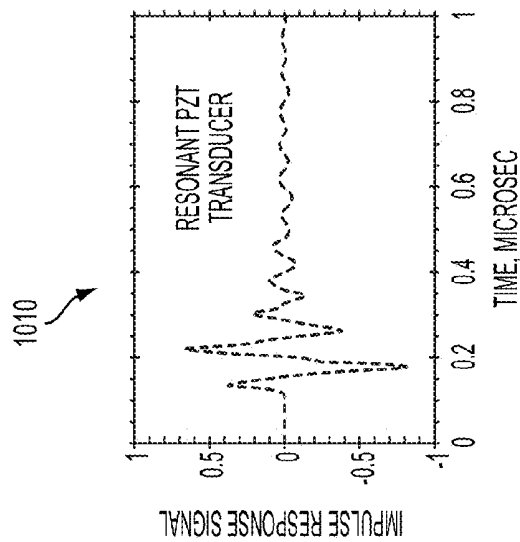


FIG. 10A

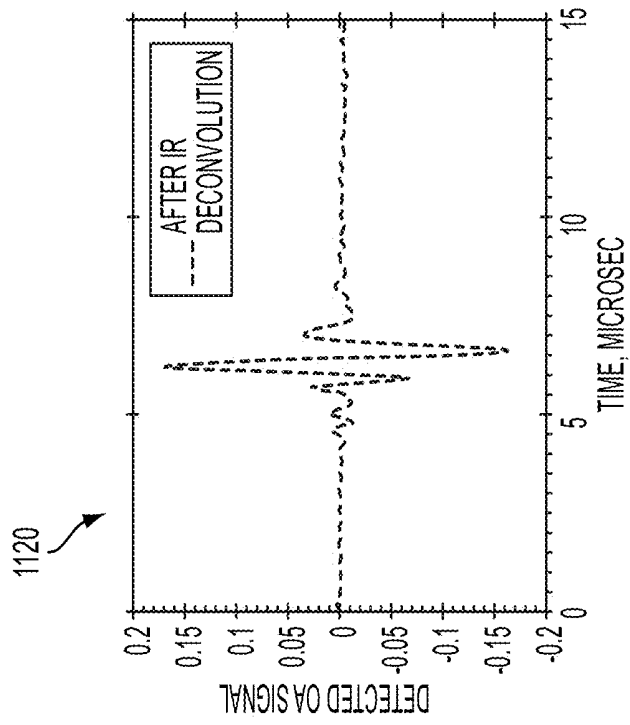


FIG. 11B

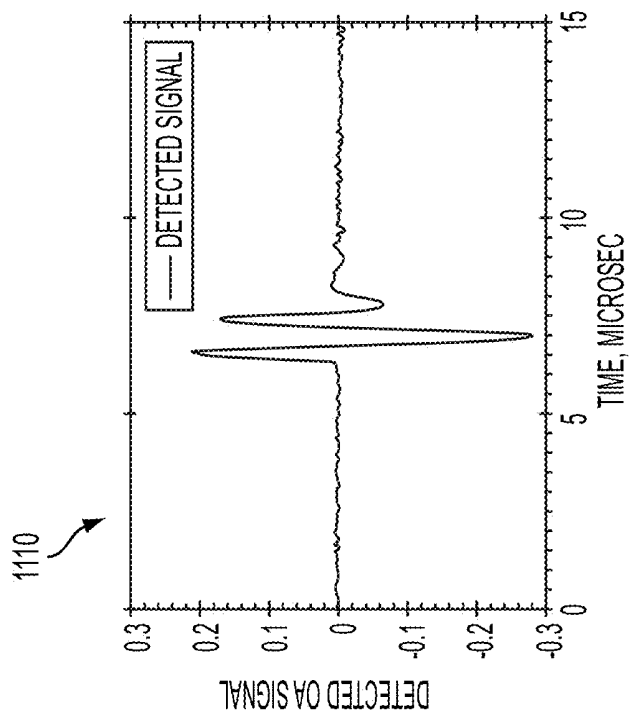


FIG. 11A

1210

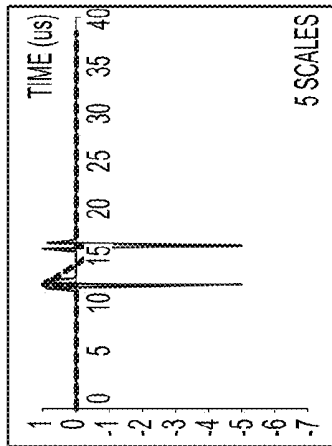


FIG. 12A

1220

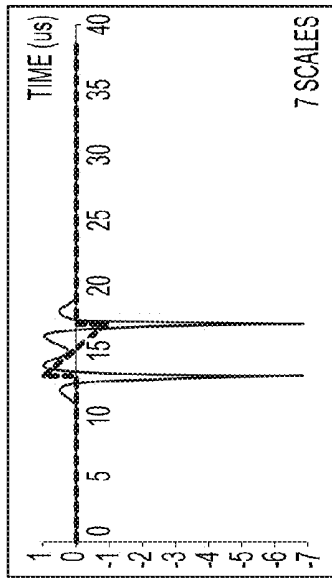


FIG. 12B

1230

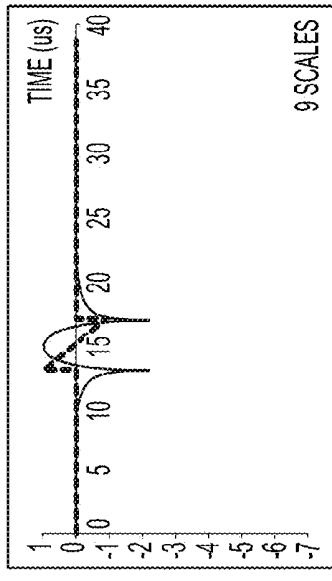


FIG. 12C

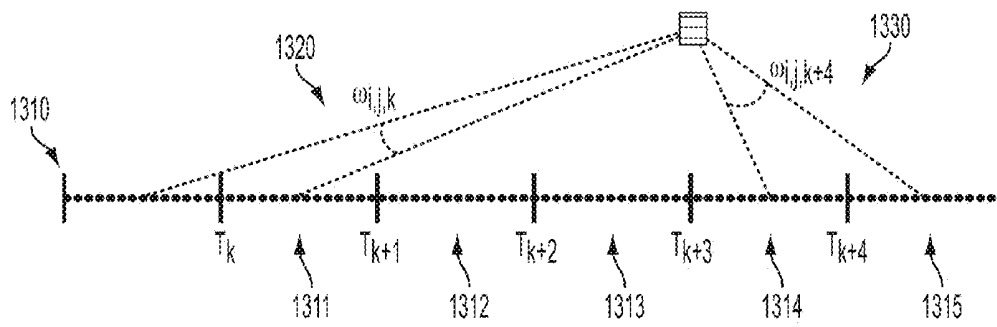


FIG. 13

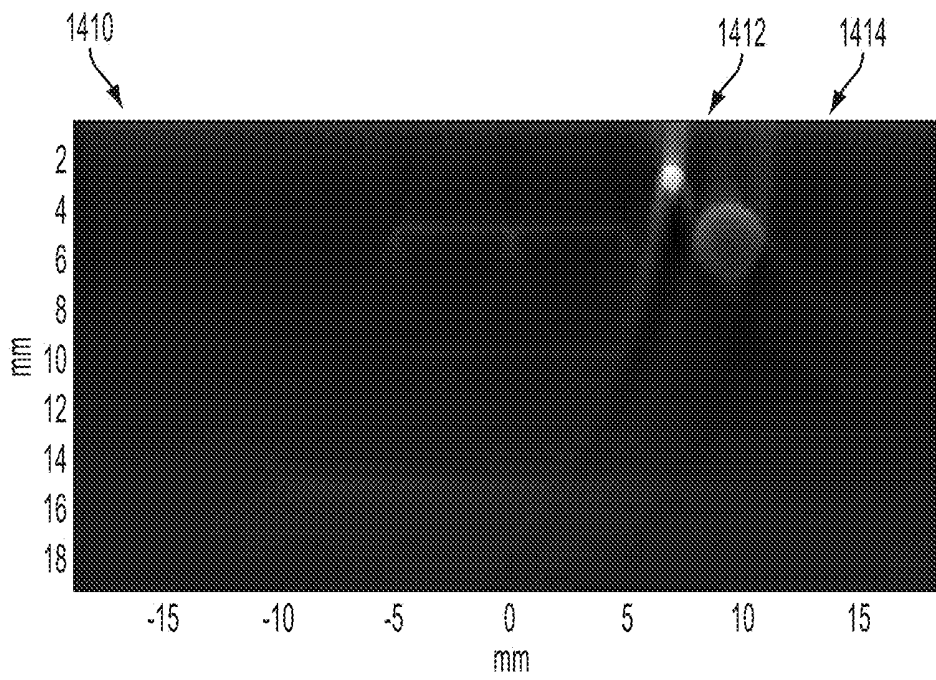


FIG. 14A

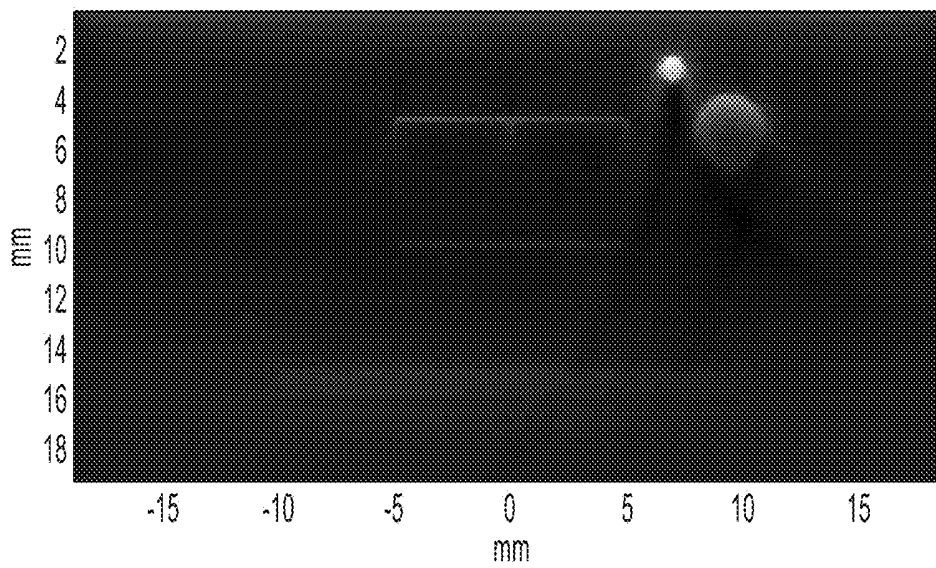


FIG. 14B

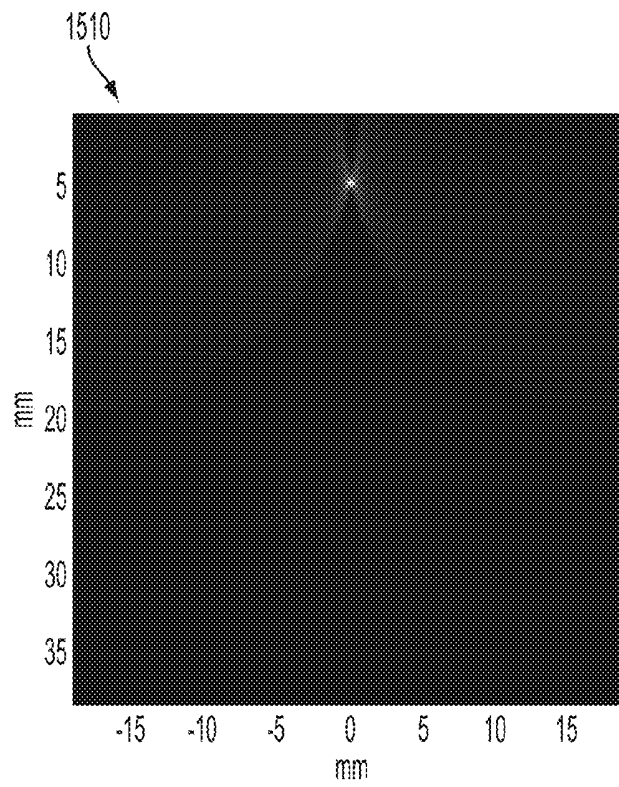


FIG. 15A

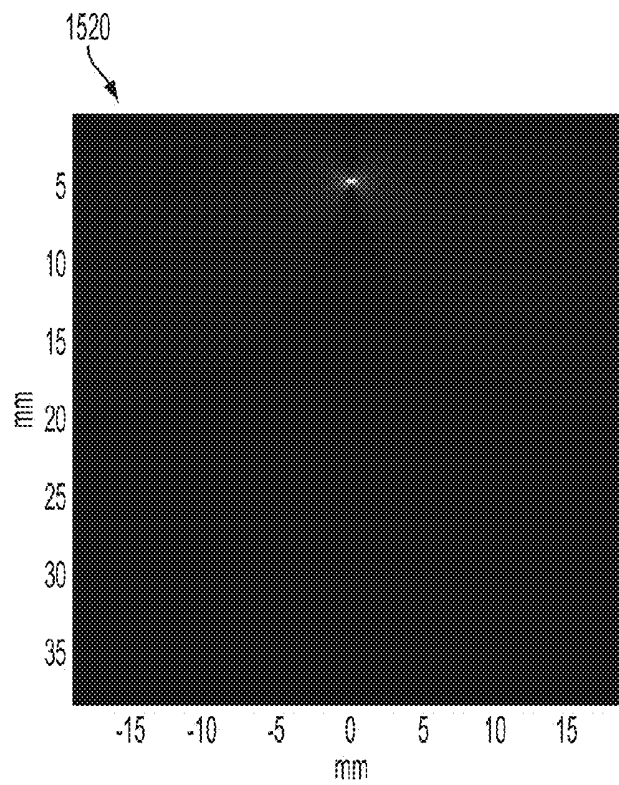


FIG. 15B

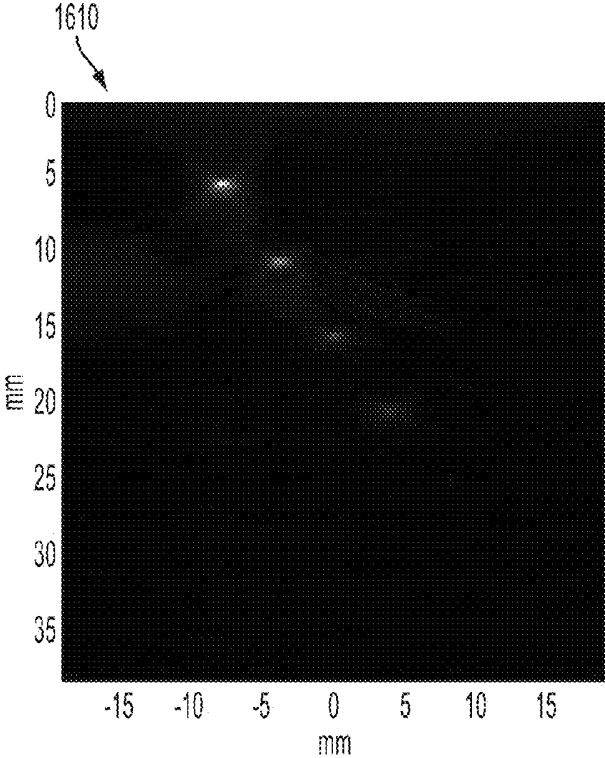


FIG. 16A

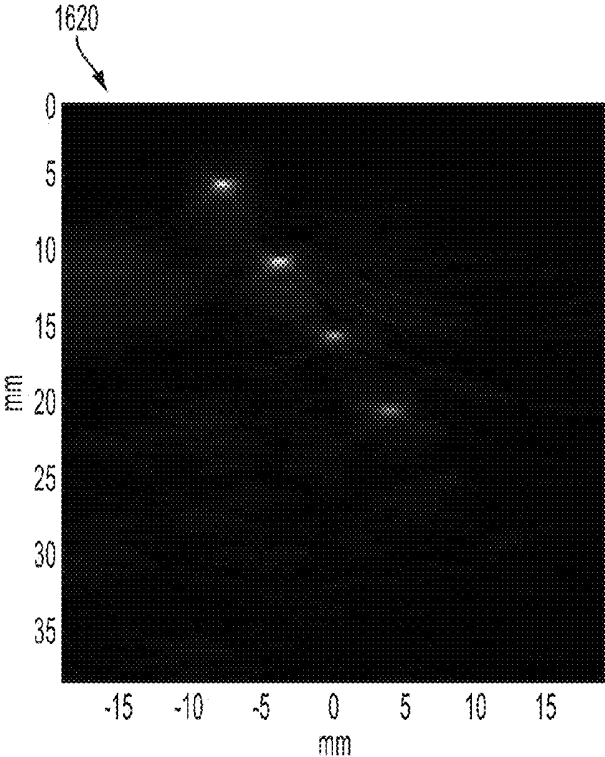


FIG. 16B

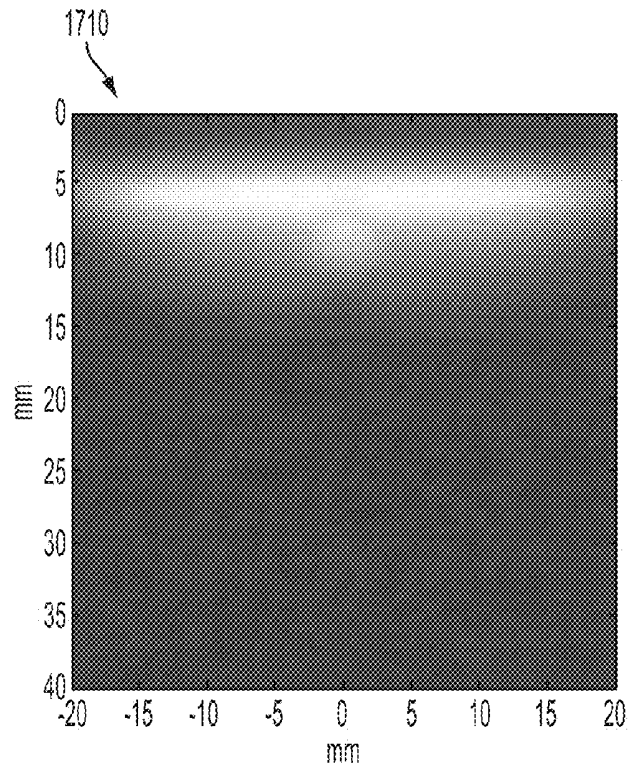


FIG. 17A

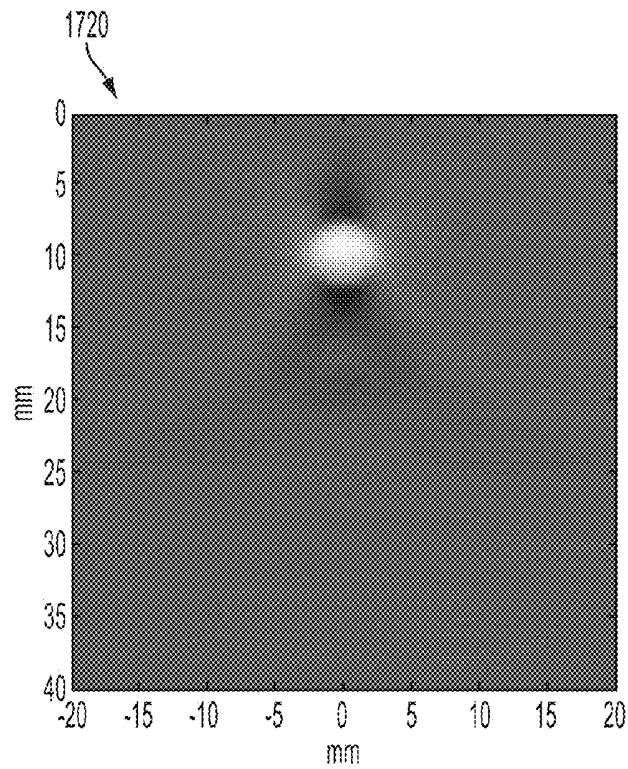


FIG. 17B

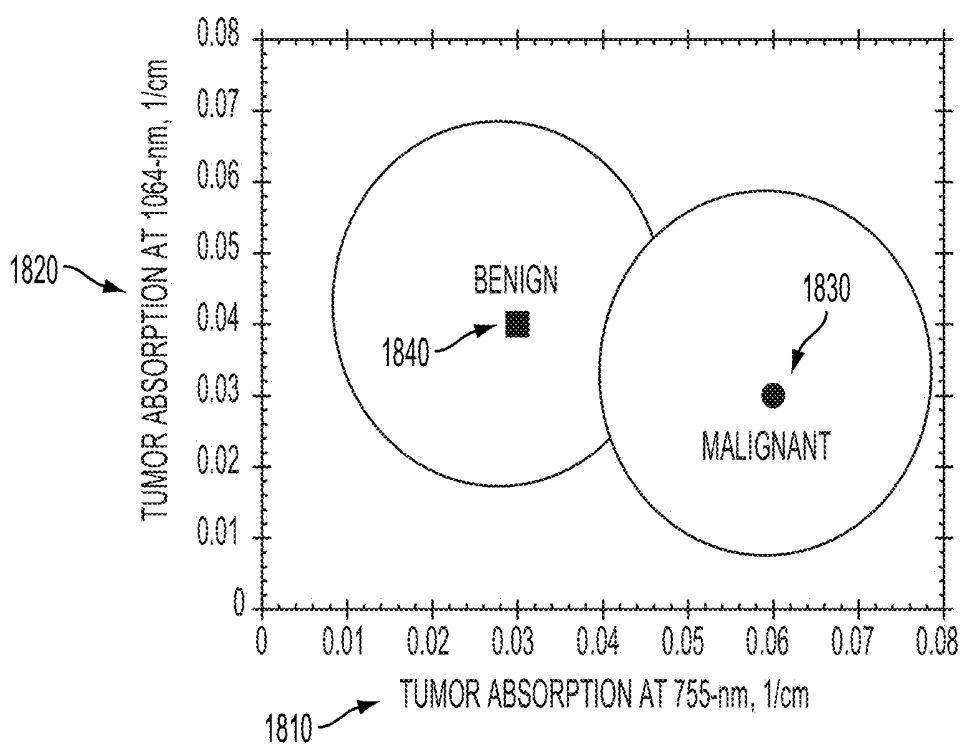


FIG. 18

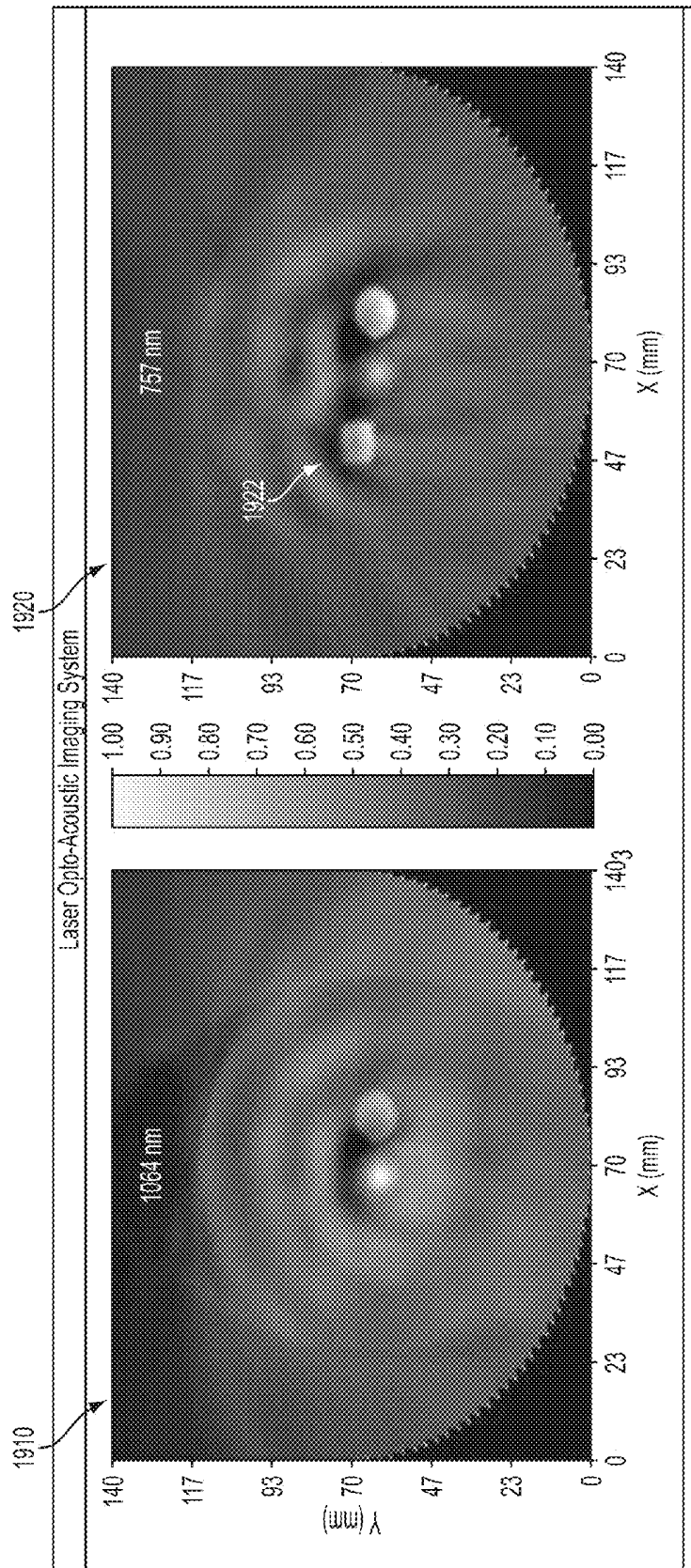


FIG. 19

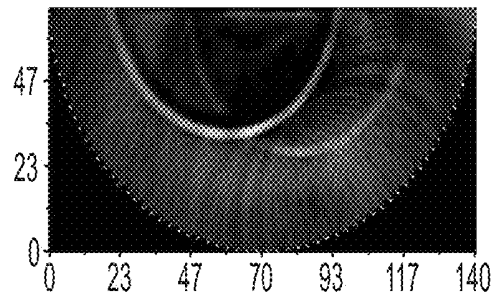


FIG. 20A

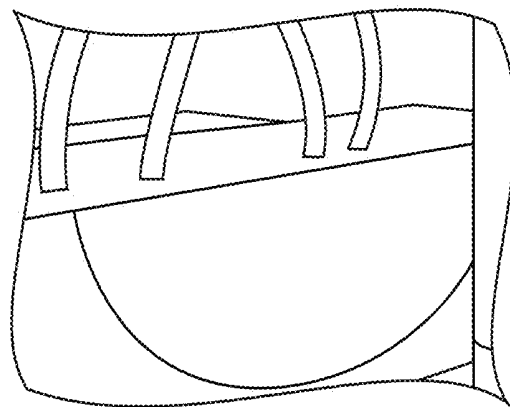


FIG. 20B

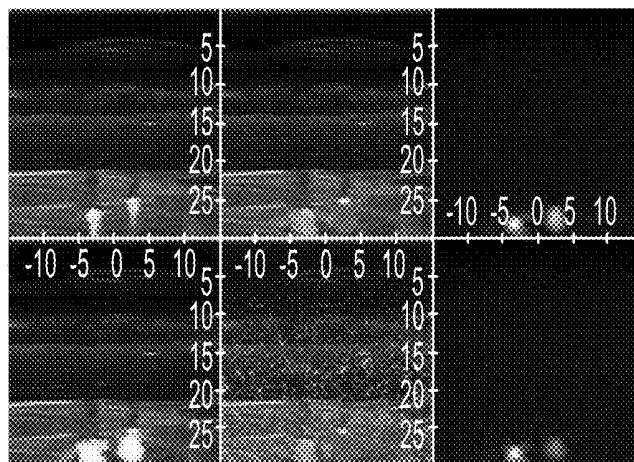


FIG. 20C

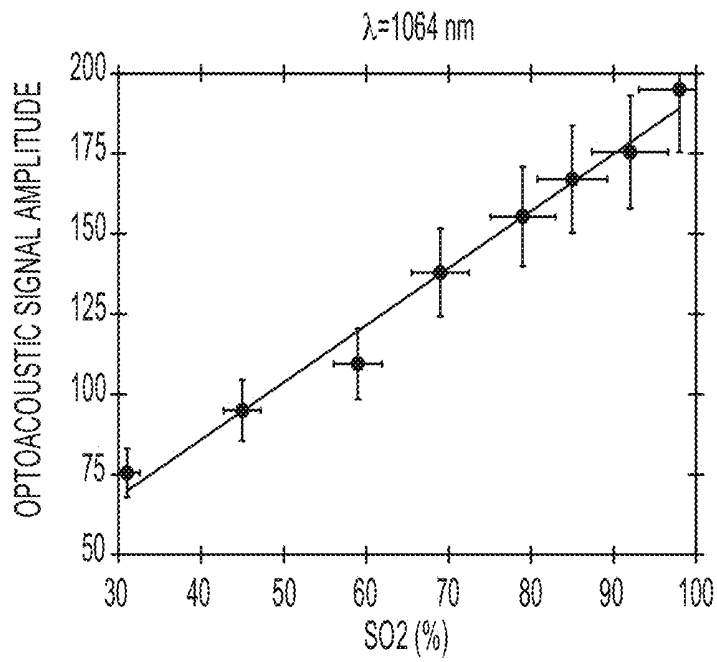


FIG. 21A

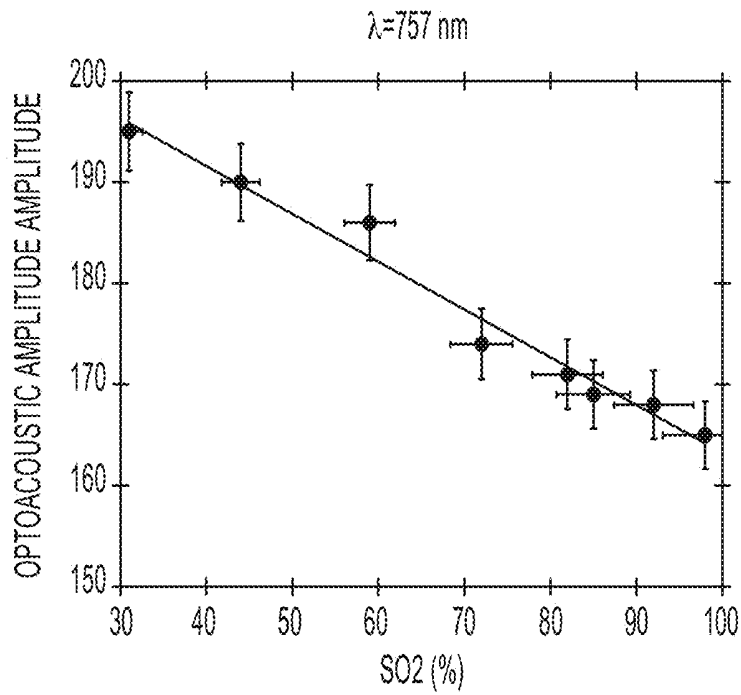


FIG. 21B

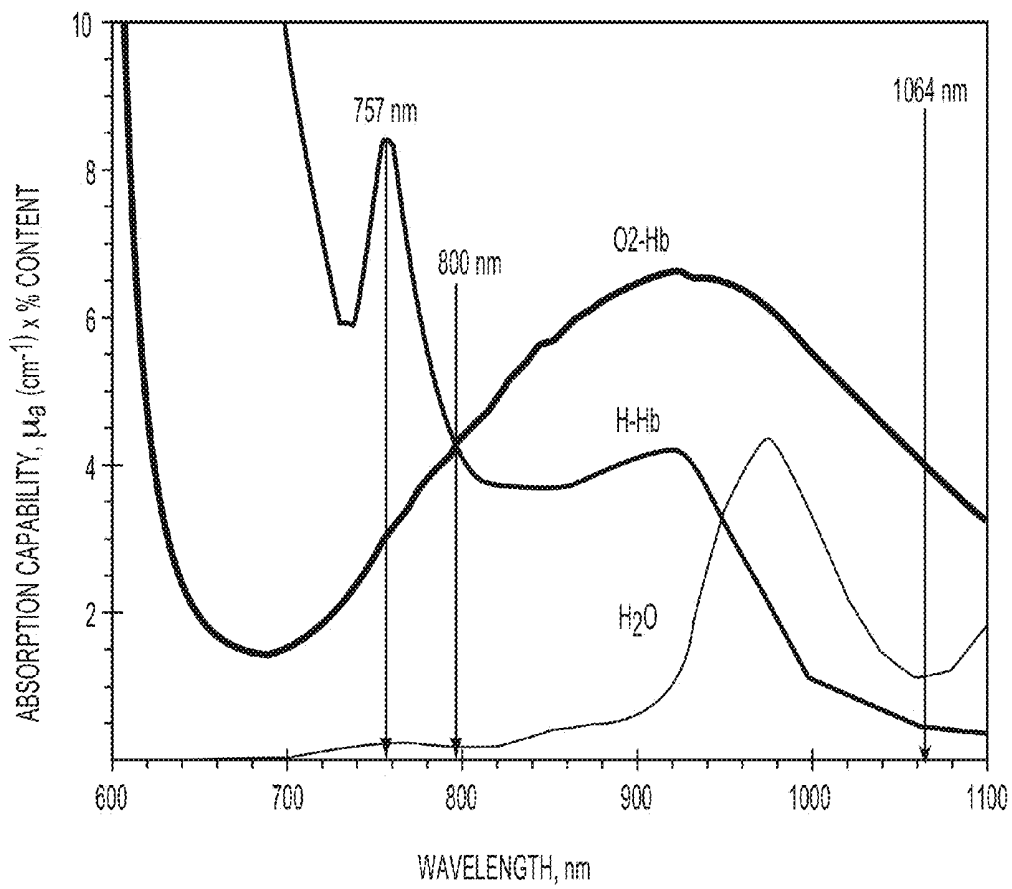


FIG. 22

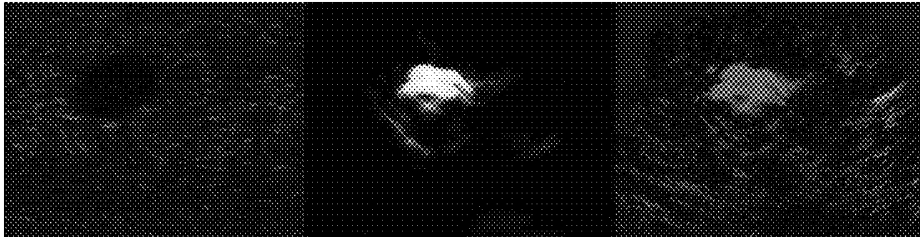


FIG. 23A

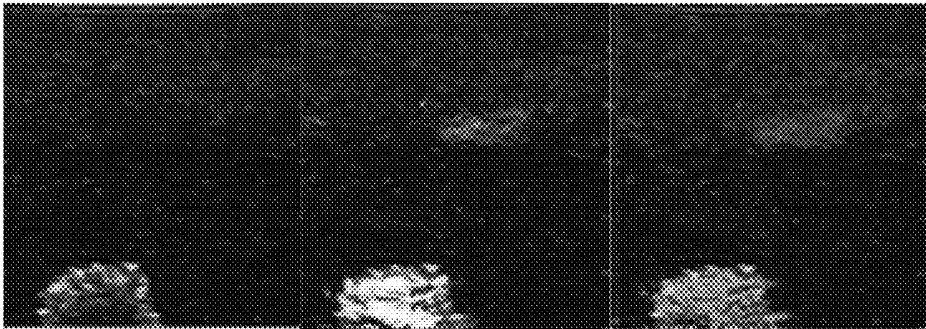


FIG. 23B

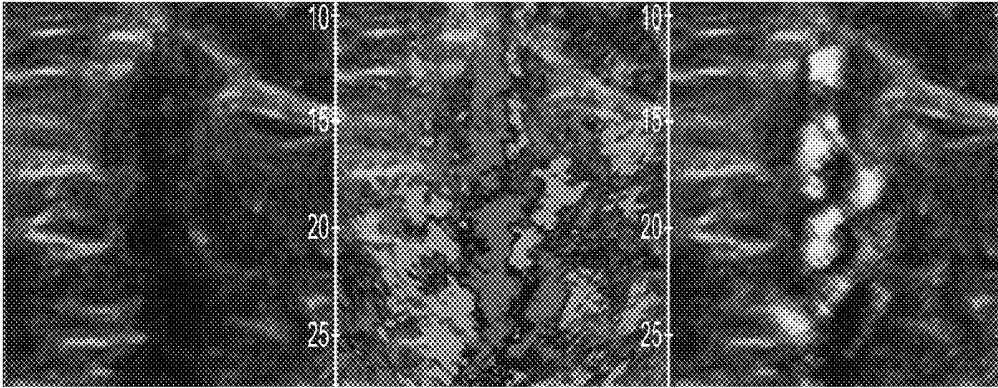


FIG. 24A

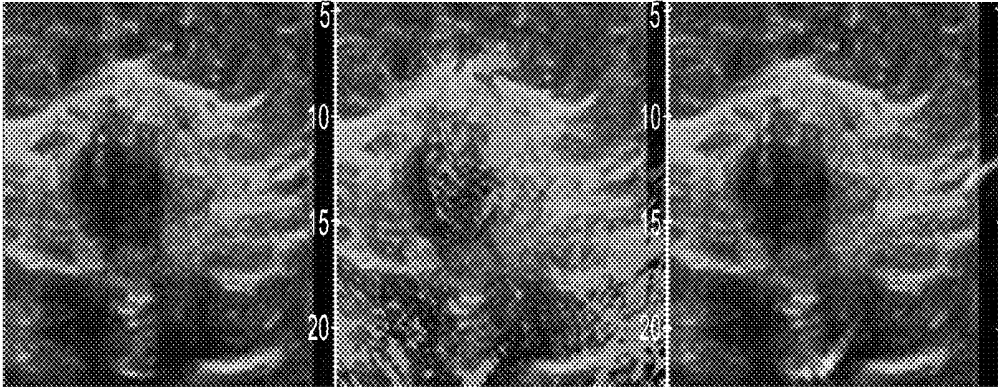


FIG. 24B

METHOD FOR DUAL MODALITY OPTOACOUSTIC IMAGING

This application is a continuation-in-part of U.S. patent application Ser. No. 13/507,217, filed Jun. 13, 2012, entitled "System and Method for Acquiring Optoacoustic Data and Producing Parametric Maps Thereof" and is a continuation-in-part of U.S. patent application Ser. No. 13/341,950, filed Dec. 31, 2011, entitled "System and Method for Adjusting the Light Output of an Optoacoustic Imaging System" and is a continuation-in-part of U.S. patent application Ser. No. 13/287,759, filed Nov. 2, 2011, entitled "Handheld Optoacoustic Probe." The entire disclosures of those applications, including the appendices thereof, are incorporated herein by reference.

FIELD OF THE TECHNOLOGY

At least some embodiments disclosed herein relate, in general, to systems for biomedical imaging, and more particularly, to real-time imaging systems that visualize thin tissue slices noninvasively through skin.

BACKGROUND

Medical ultrasound imaging is a well-established imaging technology for visualization of tissue morphology in various organs that provides diagnostic information based on analysis of anatomy. Optoacoustic imaging is used in medical applications for in vivo and in vitro mapping of animal and human tissues and organs based on variation in tissue optical properties. Optoacoustic tomography can provide anatomical, functional and molecular imaging, but the most significant value of optoacoustic imaging is in its capability to provide quantitative functional information based on endogenous contrast of molecular constituents of red blood cells. The essence of functional imaging is to provide the physician with a map of blood distribution and its level of oxygenation, so that the physician can determine whether particular tissue functions normally or not. For example, a map of total hemoglobin distribution simultaneously showing an area with increased concentration and decreased oxygen saturation indicates potential malignancy. The essence of molecular imaging is to provide maps of distributions and concentrations of various molecules of interest for a specific health condition. For example, distribution of specific protein receptors in cell membranes gives insight into molecular biology or cells that aids in designing drugs and therapeutic methods to treating human diseases.

SUMMARY

In an embodiment, the invention provides a real-time imaging system that visualizes thin tissue slices noninvasively through skin and provides three independent and co-registered images with biomedically significant information. Specifically, images of deep biological tissue structures are precisely superimposed with images of tissue functional state, such as the total hemoglobin concentration and blood level of oxygen saturation. The invention in this embodiment thus combines ultrasonic imaging and optoacoustic imaging technologies in a novel manner. These technologies can advantageously be combined given the complementary nature of information provided by them, and the fact that the same set of ultrasonic/pressure detectors and the same set of analog and digital electronics can be used to acquire both types of signals from tissues. In order to achieve a high level

of accuracy of quantitative information and present it substantially in real time (i.e. substantially as it occurs), a design is disclosed that utilizes one or more dual-wavelength short-pulse lasers or a plurality of single-wavelength short pulse lasers, a fiberoptic light delivery system, a hand-held imaging probe, other electronic hardware and processing software.

In an embodiment, an imaging system is disclosed for visualization of slices into the depth of tissue of at least a portion of a body. The system includes a processing subsystem that produces three independent images, including two functional images showing distribution of the total hemoglobin concentration and distribution of the blood oxygen saturation and one morphological image of tissue structures, the images being co-registered in time and space by utilizing one and the same hand-held imaging probe. The system may include a three-dimensional positioning system which provides the capability of assembling three dimensional volumetric images of said body from two-dimensional slices made through the depth of tissue obtained by scanning a hand-held probe along the surface of at least portion of the body.

In an embodiment, an imaging method provides coregistered functional and anatomical mapping of tissue of at least a portion of a body. Ultrasonic pulses are delivered into the tissue and backscattered ultrasonic signals reflected from various structural tissue boundaries associated with body morphology are detected. Two optical pulses having different spectral bands of electromagnetic energy are delivered, and transient ultrasonic signals resulting from selective absorption of different energy fractions from each of the two optical pulses by hemoglobin and oxyhemoglobin of blood containing tissues are detected. Detected ultrasonic signals are processed to remove noise, to revert signal alterations in the course of signal propagation through tissue and through the detection system components, and to restore the temporal shape and ultrasonic spectrum of the original signals. Image reconstruction and processing is performed to generate morphological images of tissue structures coregistered and superimposed with partially transparent functional images of the total hemoglobin concentration and blood oxygen saturation. The above steps of the process are repeated with a video frame rate so that real-time images can display tissue functional and morphological changes substantially as they occur.

BRIEF DESCRIPTION OF THE DRAWINGS

The disclosed embodiments are illustrated by way of example and not limitation in the figures of the accompanying drawings in which like references indicate similar elements.

FIG. 1A illustrates an embodiment of an optoacoustic probe with illumination of tissue through skin by a scattered light beam formed in tissue by merging two optical beams.

FIG. 1B illustrates how laser illumination light and an acoustic signal from an optoacoustic probe can be scattered from the skin towards an acoustic lens of a probe.

FIGS. 2A and 2B illustrate optoacoustic signals showing the impact of lateral ultrasonic waves induced by laser pulses in skin using optical beams on each side of an ultrasound transducer array, and using detection by transducers tilted at large angle relative to the plane of images generated therefrom.

FIG. 3 illustrates an embodiment of manifestation of image artifacts associated with the edge effect of optical illumination beam having abrupt changes of the optical fluence.

FIGS. 4A-4C illustrate embodiments wherein optical illumination of tissue is accomplished using a hand-held optoacoustic probe that delivers optical energy from either under the optoacoustic probe or on the side of the probe at different distances.

FIGS. 5A and 5B illustrate two embodiments of a hand-held optoacoustic ultrasonic probe protected from optical illumination of the acoustic lens.

FIG. 6 illustrates optoacoustic images using a probe with an acoustic lens that is not totally optically reflective and with a probe having an optically reflective layer of gold, which removes lens related image artifacts.

FIG. 7A illustrates an embodiment of an optical beam with sharp edges that may produce edge effects of acoustic waves and related artifacts and an optical beam with smooth edges producing reduced edge-related artifacts.

FIGS. 7B and 7C illustrate designs of an output fiber bundle with multiple sub-bundles shaped to provide even illumination of the image plane and reduce edge related optoacoustic artifacts.

FIG. 8 illustrates the effect of optical illumination for two probes where two fiber bundles on each side of the respective probes are oriented to illuminate skin directly under the probe.

FIG. 9A illustrates embodiments of ultrasonic probes having flat, concave or convex arc shapes.

FIG. 9B shows a hand-held optoacoustic probe having a concave arc shape.

FIG. 9C illustrates details of a hand-held optoacoustic probe having a concave arc shape.

FIG. 9D shows an optoacoustic image of three spherical objects and demonstrates that within the field of view of the arc spatial (and especially lateral) resolution is excellent even for a large object.

FIG. 9E illustrates an alternate embodiment of an optoacoustic/ultrasonic hand-held probe design.

FIGS. 10A-10C show examples of the impulse response of an ultrasonic transducer with a relatively narrow ultrasonic frequency band of sensitivity, the impulse response of an ultrawide-band ultrasonic transducer, and the ultrasonic spectra of transducer sensitivity as a function of frequency for ultrawide-band and narrow band resonant transducers.

FIGS. 11A-11B provides an illustrative example of the deconvolution of impulse response of transducers from the detected optoacoustic signals where deconvolution restores the original, unaltered, N-shaped pressure signals.

FIGS. 12A-12C provide an illustrative example of wavelet filtered N-shaped optoacoustic signals restored to their original rectangular pressure profile by summation of all scales corresponding to frequency ranges from low to high for five scales, seven scales and nine scales.

FIG. 13 provides an illustrative diagram of radial back-projection where each transducer element aperture is weighted and normalized for the total aperture of the transducer array.

FIGS. 14A and 14B provide an illustrative example of optoacoustic tomographic images of an imaging slice through tissue with a small artery, larger vein and a rectangular grid allowing estimation of system performance in visualization of microvessels.

FIGS. 15A and 15B provide an illustrative example of optoacoustic tomographic images of a point spread function

as visualized with a flat linear probe using a backpropagation algorithm and an aperture normalized backprojection algorithm.

FIGS. 16A and 16B provide an illustrative example of optoacoustic images of a phantom with hairs embedded at different depths where the first image was created using an embodiment of a standard palette and the second image was created using an embodiment of a depth-normalized palette.

FIGS. 17A and 17B provide an illustrative example of optoacoustic images of a phantom of a spherical simulated tumor obtained with a flat linear probe.

FIG. 18 shows a diagram illustrating tumor differentiation based on absorption coefficients at two wavelengths, 757 nm and 1064 nm, which match the local maximum of hemoglobin absorption like in totally in hypoxic blood (757 nm) and minimum of the ratio of absorption by hypoxic hemoglobin to absorption by oxyhemoglobin like in normally oxygenated blood (1064 nm).

FIG. 19 illustrates tumor differentiation based on absorption coefficients at two wavelengths in a phantom simulating benign (box) and malignant (sphere) tumors.

FIG. 20A shows an optoacoustic image of two intersecting tubes filled with blood having different levels of blood [SO₂].

FIG. 20B shows a photograph of an experimental setup that includes artificial blood vessels placed in milk solution and imaged using arc-shaped optoacoustic probe.

FIG. 20C shows coregistered 2D cross-sectional anatomical and functional images of blood vessel tubes showing six image panels with different anatomical and functional images.

FIGS. 21A and 21B show optoacoustic signal amplitude as a function of blood oxygen saturation (with constant hematocrit) under laser illumination at a wavelength of 1064 nm in FIG. 21A and at 757 nm in FIG. 21B. These plots illustrate that blood oxygen saturation can be monitored with optoacoustic imaging.

FIG. 22 illustrates optical absorption spectra of the main tissue chromophores absorbing optical energy in the near-infrared range: hemoglobin, oxyhemoglobin and water.

FIGS. 23A and 23B illustrate coregistered functional and anatomical imaging of breast tumors in phantoms accurately replicating optical and acoustic properties of an average breast with tumors.

FIGS. 24A and 24B illustrate coregistered functional and anatomical imaging of breast tumors.

DETAILED DESCRIPTION

The following description and drawings are illustrative and are not to be construed as limiting. Numerous specific details are described to provide a thorough understanding. However, in certain instances, well-known or conventional details are not described in order to avoid obscuring the description. References to one or an embodiment in the present disclosure are not necessarily references to the same embodiment; and, such references mean at least one.

Reference in this specification to “an embodiment” or “the embodiment” means that a particular feature, structure, or characteristic described in connection with the embodiment is included in at least an embodiment of the disclosure. The appearances of the phrase “in an embodiment” in various places in the specification are not necessarily all referring to the same embodiment, nor are separate or alternative embodiments mutually exclusive of other embodiments. Moreover, various features are described which may be exhibited by some embodiments and not by

others. Similarly, various requirements are described which may be requirements for some embodiments but not other embodiments.

System Overview

In at least some embodiments, the present disclosure is directed to a dual-modality ultrasonic/optoacoustic system for medical diagnostics that uses a hand-held probe for scanning along the skin surface of an organ and provides two types of two-dimensional maps into the depth of tissue, anatomical (morphological) and functional (blood hemoglobin index and blood oxygenation index). In an embodiment, these two maps are spatially coregistered by using the same array of ultrasonic transducers and temporally coregistered by acquiring the two types of images in real time, faster than any physiological changes can occur in the tissue of diagnostic interest. The blood hemoglobin index represents blood hemoglobin concentration changes in the areas of diagnostic interest relative to the background blood concentration. The blood oxygenation index represents blood oxygenation changes in the areas of diagnostic interest relative to the background level of blood oxygenation. These coregistered maps can be used to noninvasively differentiate malignant tumors from benign lumps and cysts.

In an embodiment, the dual-modality ultrasonic/optoacoustic system of the present disclosure provides two-dimensional imaging of a body utilizing delivery of optical energy and acoustic detection of resulting transient pressure waves using interchangeable hand-held probes, one of which is flat and used to perform a translational scan through at least a flat portion of the body under examination, and the second of which is curved being shaped as a concave arc to perform a translational scan through at least a cylindrical or curved portion of the body under examination, both scans contribute to a more complete understanding normal or pathological functions in the body.

In an embodiment, at least a portion of the body under examination contain molecules of blood constituents such as hemoglobin and oxyhemoglobin responsible for body functions or receptors in cells responsible for cell functioning, water, lipids or other constituents.

In an embodiment, optical energy produced using at least one laser beam is used for body illumination with at least one wavelength of light. In an embodiment, the optical energy is pulsed, with the pulse duration shorter than the time of ultrasound propagation through the distance in the body equal to the desirable spatial resolution. In an embodiment, the optical energy is within the spectral range from 532 nm to 1064 nm. In an embodiment, the optical energy is replaced with other electromagnetic energy with the wavelength from 1 nm to 1 m.

In an embodiment, electronic signals produced by ultrasonic transducers are amplified using low noise wide band electronic amplifiers with high input impedance. In an embodiment, analog electronic signals are digitized by a multi-channel analog-to-digital converter and further processed utilizing a field programmable gate array. In an embodiment, the ultrasonic transducers are ultrawide-band transducers that detect ultrasonic signals with no or minimal reverberations. In an embodiment, the system is integrated with an ultrasound imaging system used to enhance visualization of acoustic boundaries in the body and parts of the body with different density and/or speed of sound.

In an embodiment, quantitative measurements of concentrations of target molecules, cells or tissues is made through characterization of optical energy propagation and absorption combined with processing of digital electronic signals by deconvolution of the hardware transfer function in order

to obtain intrinsic optoacoustic amplitude and profile of such signals and the distribution of the optical absorption coefficient in the body.

In an embodiment, an optoacoustic contrast agent is used to visualize a portion of the body of interest or characterize distribution of certain molecules, cells or tissues in the body.

In an embodiment, the system comprises at least a laser, a light delivery system, an optoacoustic probe, an electronic system, a computer and an image display.

Laser

In an embodiment, the laser is capable of emitting short, nanosecond pulses of near infrared light at two (or more) different toggling wavelengths, i.e. two different spectral bands. In an embodiment, one of the wavelengths is preferentially absorbed by hemoglobin of blood and the other is preferentially absorbed by oxyhemoglobin of blood. In an embodiment, illumination of the organ under examination with the first laser pulse at one wavelength (spectral band) and detection of the first optoacoustic signal profile resulting from the first illumination, followed by the illumination with the second laser pulse at the second wavelength band and detecting of the second optoacoustic signal profile, can provide data that can be used for reconstruction of two coregistered tomographic images that can be used for generation of functional maps of the areas of diagnostic interest based on (i) blood hemoglobin index and (ii) blood oxygenation index.

Light Delivery System

In an embodiment, the light delivery system comprises bundles of optical fibers. In an embodiment, the input of the optical fiber bundle is circular to match the incident laser beam, while the output of the fiber bundle is rectangular to match the size and shape of the ultrasonic transducer array. In an embodiment, each fiber has a small diameter (e.g., down to 50 micron) to provide excellent flexibility of the bundles. In an embodiment, the input tip of the fiber bundle is fused to shape the bundle into a hexagon and to eliminate spaces between the fibers in the bundle, thereby providing up to 20% better transmission of the laser energy. In an embodiment, the output tip of the fiber bundle is fully randomized such that fibers that appear close to each other at the input will appear far from each other at the output or even in different branches of the bifurcated fiber bundle.

Optoacoustic Probe

The probe is designed to provide high contrast and resolution of both optoacoustic and ultrasonic images. In an embodiment, the probe is a hand-held probe with an array of ultrasonic/optoacoustic transducers, which can be designed to be single dimensional, 1.5 dimensional or two-dimensional. In an embodiment, the transducers detect acoustic waves within an ultra-wide band of ultrasonic frequencies and the ultra-wide band is shaped to match the spectrum of optoacoustic signals emitted by tissue of diagnostic interest. In an embodiment, the transducers are also designed to emit acoustic waves as short pulses of ultrasound with short ring-down time and minimal reverberations of gradually decreasing magnitude.

To achieve such a design, transducer material can be chosen from, for example, piezoelectric ceramics (such as PZT, PMN-PT, and PZNT), piezoelectric single crystals (such as PZT, PMN-PT, and PZNT), piezoelectric polymers (such as PVDF and copolymer PVDF copolymer), composite polymer-ceramic and polymer-crystal piezoelectric materials and capacitive micromachined ultrasonic transducers (CMUT). In an embodiment, the thickness of the transducer

elements that provide the central frequency and materials of the backing layer and the front surface matching layer of the transducers are optimized.

In various embodiments, the shape of the ultrasound transducer array may be either flat or concave arc. A flat design is suited to scanning of the surface of an organ under examination that has radius of curvature much larger than the size of the probe, such as a human body. A concave arc-shaped design provides the largest aperture for the optoacoustic signal detection with minimal physical dimensions. The large aperture, in turn, provides for improved lateral resolution within the angle of the field of view formed by lines connecting the arc's focal point with each edge transducer of the array. The arc-shaped probe is often the most effective for scanning body surfaces that are curved with a radius approximately matching that of the probe (such as the average sized breast, neck, arms and legs).

FIG. 1A illustrates an embodiment of an optoacoustic probe that provides illumination of tissue (TS) through skin (SK) by the scattered light (SL) beam formed in tissue by merging two optical beams (OB) emerging from fiber bundles (FB) expanding and passing through light diffusers (LD) then passing through optical windows (OW). Acoustic waves (AW) generated in blood vessels or tumors (BV or TM) by the scattered light (SL) in tissue propagate through acoustic lens (AL) to transducers (TR) and converted into electrical signals being transmitted by electrical cables (EC) through the backing material (BM) to the electronic amplifiers.

In an embodiment, the design of the optical fiber bundle is as follows. The input of the fiber bundle is circular with fused fiber tips to avoid loss of light through spaces between the fibers. The fiber diameter may be approximately 200 microns for good flexibility, and a fiber diameter of 100 microns or even 50 microns may be desirable in a particular application. This fiber bundle is Y-split into two half-bundles and fully randomized, so that substantially any two neighboring fibers from the input appear in different half-bundles. At least a majority of the neighboring fibers should be randomized in this regard. Each half-bundle is preferably split into multiple sub-bundles, and each sub-bundle is placed in its slot/niche to form fiber bundle "paddles". The two paddles are placed on each side of the ultrasonic transducer (TR) array assembly. As is discussed below with reference to FIGS. 7B and 7C, the output shape of each fiber bundle paddle may be rectangular for the width of the field of view, typically 40 mm, and have triangular shaped ends. Such triangular shape allows the output beam to have smooth edges after passing through light diffuser (LD), FIG. 1A. Finally, the optical beam from fiber bundle paddles exit from the probe into the skin (SK) through optical windows (OW) that comprise thin anti-reflection-coated glass plates or anti-reflection-coated polymer or plastic plates with acoustic impedance matching that of tissues to be imaged.

There are a number of objectives for the present optoacoustic probe design: (i) substantially no light should propagate either through the acoustic lens (AL) or through the optical block acoustic damper (OBAD) on the sides of the probe, (ii) substantially no acoustic waves should be generated in the acoustic lens or the optical block acoustic damper materials through absorption of light; acoustic waves in a wide range of ultrasonic frequencies from 0.1 MHz to 15 MHz should be able to pass through (AL) with no attenuation, and no acoustic waves should be able to pass through OBAD; (iii) the optical beams (OB) exiting through optical windows (OW) should have smooth edges of the optical fluence, and these optical beams should enter the skin

as close to each other as necessary to merge due to optical scattering within the skin and enter underlying tissue under the array or transducers providing maximum fluence in the image plane.

In an embodiment, the light delivery system directs light underneath the transducer elements, not through the array of transducer elements. In an embodiment, the design of the optoacoustic probe is based on an array of ultrasonic transducers with fiber optic delivery systems on each side of the ultrasonic array, positioned as close to the transducers as possible and with dimensions in the elevation axis of the transducer as small as possible, considering the need to focus ultrasonic beams to the depth of the most probable target. In an embodiment, the fiber optic delivery system is designed to allow penetration of the optical energy of the near infrared light into the organ being imaged, such as a breast, and minimum opto-thermo-mechanical interaction of the light beam with skin.

Another alternative design of the light delivery system delivers light to a mirror or prism(s) placed underneath of the ultrasonic transducers in order to reflect the light orthogonally to the skin surface of an organ being imaged. In such embodiments, a standoff can be placed between the transducer elements and the skin/tissue. These alternative embodiments may be combined within the scope of the invention.

Detailed Description of Aspects of System Components Optical Illumination and Probe Design

An acoustic lens is typically placed on transducers within an optoacoustic probe for purposes of focusing ultrasonic beams. While a probe could be provided without an acoustic lens, if there is no lens then ultrasonic transducers may be directly exposed to light and absorb such light, which can result in very large artifact ultrasonic signals, especially where such light is pulsed. Optical illumination of the lens on an ultrasonic probe causes very strong transient acoustic waves that result in image artifacts. Up to 50% of near infrared light can be diffusely scattered by skin, depending on skin color. Mismatch of acoustic impedance between the lens of the transducer elements can cause reverberations with long ring down time. Therefore, an embodiment of a probe design includes a white strongly scattering opaque lens. If such lens is not needed due to curved shape of each transducer element, then a white strongly scattering front matching layer should be employed to protect transducer elements from near-infrared light.

FIG. 1B illustrates how laser illumination light 110 and 120 from an optoacoustic probe can be scattered 130 from the skin 140 towards an acoustic lens 150 of a probe.

Furthermore, (laser) optical pulses can have a direct impact on ultrasonic transducers of the acoustic waves induced by strong interaction of the optical pulses with skin of the organ being imaged that laterally traverse along the skin surface in a direction orthogonal to the image plane. When detected by the array of transducers, spatial distributions of these acoustic waves are projected onto the optoacoustic image at a depth equal to the lateral distance between the array of transducers and the optical beams on the skin surface, creating artifacts. Furthermore, acoustic waves generated in skin through reverberation of the acoustic lens and the housing of the probe can further affect the quality of imaging.

FIGS. 2A and 2B illustrate exemplary optoacoustic signals showing impact of lateral ultrasonic waves induced by laser pulses in skin using optical beams on each side of an ultrasound transducer array. The signals shown are generated by transducers in the direction almost orthogonal to the

plane of images generated therefrom. Such transducers may receive signals at large oblique angle (up to 90 deg) relative to the plane of images generated therefrom, which is undesirable. Therefore, the design of the transducer array includes means to reject signals coming out of the image plane. Such means include but not limited to concave arc shape of the transducer elements and acoustic lens and delivery of the optical beam underneath the transducers. The detected optoacoustic signals **210** in FIG. 2A were generated using an effective acoustic coupling agent, in this case water. The signals **220** in FIG. 2B were generated in the absence of such acoustic coupling agent, i.e., using only air space to couple the acoustic signals to the transducer array.

Furthermore, the finite dimensions of the optical beam can affect the acoustic waves generated in response to impingement of the optical beam on tissue. Such acoustic waves can be generated at the sharp edges of the optical beam, propagate towards the array of transducers and result in artifacts. Since a system that utilizes flat linear array of ultrasonic transducers is configured such that the first and the last transducer in the array detect these waves first and the central transducers detect these waves the last, this "edge effect" results in v-shaped artifacts on a sinogram of optoacoustic signals and low frequency bulk artifacts on optoacoustic images.

FIG. 3 illustrates an example of manifestation of v-shaped artifacts **310** on a sinogram **300** of optoacoustic signals and associated artifacts **320** on optoacoustic images. Since these acoustic waves are associated with the edge effect of the optical illumination beams having abrupt changes of the optical fluence, in an embodiment, one can see a V-shaped bright signals on the sinogram and associated series of artifact waves on the opto-acoustic image.

Furthermore, the illumination geometry of optical beams projected by an optoacoustic probe can affect image quality. Where the optical beams of an optoacoustic probe are placed too far apart, this can result in a gradual transition from the dark field illumination (two separate optical beams on each side of the probe resulting in the absence of direct light under the probe in the image plane) into the bright field of illumination (one beam under the probe going into the depth of tissue along the image plane). This transition creates a problem in the image brightness map making the map not quantitatively accurate and causes artifacts at the depth equal to the initial width between separate optical illumination beams on each side of the probe.

FIGS. 4A-4C illustrate an embodiment wherein optical illumination of tissue is accomplished using a hand-held optoacoustic probe **410**, **420**, **430** that delivers optical energy from either under the optoacoustic probe or on the side of the probe at different distances. In the embodiment of FIG. 4A, when the optical beams are delivered under the ultrasonic probe, the distribution of the optical energy in the image plane has a smooth gradient with a maximum at the skin surface. This optical distribution is beneficial for high contrast of optoacoustic images. In the embodiment of FIG. 4B, when the optical beams are delivered close to a thin optoacoustic probe, the two beams can merge due to optical scattering within the skin, so that the distribution of the optical energy in tissue under the skin can be made similar to the embodiment of FIG. 4A. In the embodiment of FIG. 4C, when the optical beams are separated by a large distance, they merge only at significant depth within tissue, creating the optical distribution in the image plane with a dark zone (no light) in a subsurface layer of the tissue and a bright zone in the depth of the tissue, which is detrimental to the contrast of optoacoustic images, especially consider-

ing projection of brightly illuminated areas of skin onto the optoacoustic image plane at a depth equal to the separation distance of the two beams.

Thus, in the embodiments illustrated in FIGS. 4A-4C, the image brightness map **412**, **422** and **432** of the tissue being scanned is optimized where the illumination of the skin is directly under the probe **410**. As the distance between the center of the transducers and the center of the optical beams increases, as shown at **420** and **430**, the image brightness map **422** and **432** of the tissue being scanned becomes progressively more uneven.

Lastly, the reflection from boundaries of tissue structures (such as tumor, vessels or tissue layers) of laser-induced ultrasound waves launched into the tissue after being generated in skin, can also lead to image artifacts represented by lines, curves and overall noise.

In an embodiment, the acoustic lens of the probe is designed such that the lens reflects and scatters, but does not absorb, light from the illumination components, yet it is optically opaque. In various embodiments, such lens can be made either using strongly optically scattering material such as silicon rubber filled with titanium dioxide or barium sulfate powder, or using a thin metallic highly reflective layer such as aluminum or gold or a combination a white opaque lens material and a metal layer. In an embodiment, to avoid peel-off of the thin metallic layer from the front surface of the acoustic lens, in case of a combination of diffusely scattering material of the lens and a thin reflective layer (foil), the metallic reflective layer can be placed between the two layers of diffusely scattering material. As it is difficult to make a material with absolutely zero optical absorption, and such absorption may generate ultrasound in thermoelastic materials, the lens material can be made from thermoplastic materials having minimal thermal expansion, which produces minimal or no ultrasound in response to the absorbed optical energy.

FIGS. 5A and 5B illustrate two embodiments, respectively, of hand-held optoacoustic ultrasonic probes **510** and **520** that are protected from optical illumination of the acoustic lens. In FIG. 5A, a totally reflective opaque white lens is utilized, and in FIG. 5B a partially reflective white lens is utilized, with light reflection capability of the lens enhanced by a gold layer or coating.

FIG. 6 illustrates optoacoustic images using a probe with a non-reflective acoustic lens **610** and a probe with reflective layer of gold **620**. The probe utilizing a reflective layer of gold **620** produces an image with reduced artifacts **612** and **614**.

In an embodiment, the probe housing serves as hypo-echoic encapsulation of the probe, which means that the probe housing is made from materials that (i) do not absorb laser light (more specifically near-infrared light), but if a small absorption is unavoidable, the materials having low thermal expansion do not emit ultrasound after absorption of the laser light, (ii) strongly attenuate and dampen ultrasonic waves and do not reverberate. The transducer assembly inside the probe housing is also made of the hypo-echoic material. Alternatively, a layer of said hypo-echoic material is placed between the transducer assembly and the fiberoptic assembly to avoid generation of any ultrasound upon interaction of light with transducer assembly. In various embodiments, such materials can be chosen, for example, from white color porous and anechoic heterogeneous composites for baffles, foams, polymers, rubbers and plastics (such as CR-600 casting resin available from Micro-Mark of Berkeley Heights, NJ, or AM-37 available from Syntech Materials of Springfield, Va.), and others. In an embodiment, any such

materials are electrically non-conducting insulators to, inter alia, protect the probe from external electromagnetic emissions.

In an embodiment, the optical illumination subsystem is configured to deliver optical beams with smooth intensity edges. In an embodiment, the width of the optical beams is equal to that of the array of ultrasonic transducers within the optoacoustic probe (for example, about 5 mm) This is achieved by designing the bundle of optical fibers to have a gradually decreasing density of fibers at the edges. This design enables one to deliver laser illumination to the skin of the organ under examination so that the beam does not generate sharp edge-related acoustic waves, and such laser-induced acoustic waves do not produce V-shaped artifacts in the sinogram of optoacoustic images.

FIG. 7A illustrates an embodiment of an optical beam with sharp edges **710** that may produce edge effects of acoustic waves and related artifacts and an optical beam **720** with smooth edges producing reduced edge-related artifacts. FIGS. 7B and 7C illustrate that an optical beam with smooth edges of fluence can be produced using a fiberoptic bundle design having multiple sub-bundles and a triangular shape in each end of the fiber bundle assembly.

In an embodiment, the fiber bundle is positioned at a distance from skin that is sufficient for the optical beam to expand to a desirable width. Where the dimensions of the probe are compact, the fibers used in the fiber bundle can be selected to have a higher numerical aperture (e.g., >0.22). In an embodiment, in order to achieve better coupling of the optical beam into the skin, the beam is delivered through an optical window. In such embodiment, the optical window touches the skin, making its surface flat for better light penetration, simultaneously removing any excess of coupling gel from the skin surface being imaged. In an embodiment, the fiber bundle and the optical window are incorporated into the probe housing, so that the air gap between the fiber bundle and the window is protected.

In an embodiment, the optical window is designed is to allow minimal interactions of both the optical beam and the laser-induced acoustic waves with such window. In an embodiment, the window is very thin and made of optically transparent material with antireflection (AR) optical coating. In an embodiment, such material has anechoic acoustic properties. These anechoic acoustic properties and the fact that the illuminated skin is being depressed upon optoacoustic scanning results in dampening of ultrasonic waves laterally propagating from the laser-illuminated skin surface to the transducer array, thereby reducing associated artifacts.

In an embodiment, the probe is designed such that the optical beams are very close to the transducer elements on each side of the ultrasonic probe, which is made as thin as technologically possible. In an embodiment, the thickness of the probe is so small (e.g., 5 mm) that the light beams delivered to skin at this distance, d , from the probe center will merge into one beam within the thickness of the skin (about $z=5$ mm), and the tissue of the organ under examination receives one beam underneath the transducer elements. This is called bright field illumination. In an embodiment, the optoacoustic probe is designed such that the optical light beam is delivered to the skin directly underneath the transducer elements.

FIG. 8 illustrates the effect of optical illumination for two probes **810** and **820** where two fiber bundles on each side of the respective probes are oriented to illuminate skin directly under the probe **812** and on either side of the probe **822**. Where the skin is illuminated directly under the probe **812**, a tumor **814** is clearly discernable and there is no clutter on

the image background **816**. Where the skin is illuminated on either side of the probe **822**, the tumor is not discernable **824** and there are numerous artifacts on the image background **826**.

In an embodiment, the optical beam width is designed to deliver increased light into the slice of tissue being imaged. In an embodiment, the beam is homogeneous, such that it has a constant fluence through the beam, as a heterogeneous beam generates acoustic sources of heterogeneities, which in turn produce artifacts in optoacoustic images. The fluence level is defined by the ANSI laser safety standards for the laser illumination of skin. The beam width is limited by the capability of the optical scattering in tissue to deliver photons of light into the central slice located underneath the transducer elements (the slice being imaged). In an embodiment, the length of the optical beam is equal to the length of the transducer array. In an embodiment, the optical beam also has smooth edges, that is to say, gradually reduced fluence at the edges, since sharp edges produce strong edge artifacts on optoacoustic images.

In an embodiment, design features of the optical illumination system and optoacoustic probe of the present disclosure can be summarized in the following Table:

TABLE 1

Summary of optical illumination and probe design.	
System Feature	Advantages
Arc hand-held probe Light delivery into the imaging plane	Higher aperture - lower distortions Improves optoacoustic image contrast and decreases artifacts by increasing the ratio of useful information (from the imaging plane) to noise (outside of the imaging plane)
Optical shielding of the probe	Reduces artifacts from direct and scattered light striking the acoustic lens, probe housing, etc.
Acoustic shielding of the probe	Acoustic shielding of the probe's housing reduces artifacts (clutter) from acoustic waves propagating through the probe's housing
Using ultrawide band transducers for both ultrasound and optoacoustic imaging	Allows to have the same array working in ultrasonic and optoacoustic imaging

In various embodiments, the shape of the ultrasonic transducer array for the combined optoacoustic/ultrasonic imaging can be either flat or convex arc-shaped. In an embodiment, the probe shape for optoacoustic imaging is concave arc-shaped. Such a concave shape provides a large aperture with minimal physical dimensions, wider field of view of an object being imaged, which in turn provides for improved lateral resolution and better reconstruction of the shape of the object being imaged.

FIGS. 9A-9C illustrate embodiments of optoacoustic/ultrasonic hand-held probes having flat or concave arc shapes **910** (FIG. 9A) and a hand-held transrectal probe with a linear shape **920** (FIG. 9B). FIG. 9C illustrates details of the optoacoustic/ultrasonic hand-held probe design with its face showing ultrasonic transducers assembly, two layers of hypo-echoic light reflecting and ultrasound damping material on each side, and two optical windows for delivery of the optical beam.

FIG. 9C illustrates details of a hand-held optoacoustic probe having a concave arc shape. Electrical cables **930** are provided for bi-directional communication to and from the probe, and fiberoptic bundles **940** are provided for delivering light to the probe. An array of wide-band ultrasonic transducers **950** send and receive acoustic energy. The transducer array **950** is covered by an opaque white cylin-

drical lens (not shown for clarity purposes) that extensively scatters and reflects near-infrared light. Optical windows 960 provide optical beam outputs. In the embodiment FIG. 9C, the ultrasonic transducers within the probe may be designed so as not to be sensitive to lateral acoustic (ultra-sonic) waves and to be free of reverberations, especially in the lateral direction. This can be achieved by the selection of the piezoelectric composite material, the shape of piezocer-amic elements in the matrix and anechoic properties of the matrix. In an embodiment, the ultrasonic transducers are also designed to possess high sensitivity within an ultrawide band of ultrasonic frequencies. This in turn results in minimal reverberations that cause artifacts on optoacoustic/ultrasonic images.

FIG. 9D shows an optoacoustic image that illustrates advantages of the concave-arc shaped hand-held probe in terms of resolution in optoacoustic images. As presented in this embodiment, the shape and sharp edges of a large sphere are well depicted in cases where the object is within the field of view of the probe aperture. Outside the probe aperture resolution and accuracy of shape reproduction decreases, however remains better than those for flat linear probes of similar width.

FIG. 9E illustrates an alternate embodiment of an optoacoustic/ultrasonic hand-held probe design that is capable of two-dimensional imaging within the plane going parallel to the skin surface at various selected depths, and three-dimensional images as well.

In an embodiment, a hand-held probe that is scanned along the skin surface producing real-time two-dimensional images of tissues in the body under examination also has a component serving for accurate global 3D positioning of the probe. This design allows the imaging system to remember positions of all tissue slices and to reconstruct three-dimensional images at the end of the scanning procedure.

Electronic Data Acquisition System

In an embodiment, the present disclosure is directed to an optoacoustic imaging system having an electronic data acquisition system that operates in both optoacoustic and ultrasonic modes and can rapidly switch between such modes. In an embodiment, this is achieved with firmware that controls functions of a Field Programmable Gate Array (FPGA), the main microprocessor on the electronic data acquisition system. In an embodiment, a reprogrammable FPGA can toggle between optoacoustic and ultrasound operation modes in real-time, thus enabling co-registration of ultrasound and optoacoustic images, which can be used for diagnostic imaging based on functional and anatomical maps. In an embodiment, FPGA functions include controlling, acquiring, and storing optoacoustic and/or ultrasound data, signal processing and transferring data for real-time image reconstruction and processing. In an embodiment, the FPGA may also be employed in ultrasound beam forming and image reconstruction.

In an embodiment, the electronic data acquisition system design utilizes one or more multi-core Graphical Processor Units (GPU) for image reconstruction and processing. In the ultrasound mode, in an embodiment, the FPGA controls the ultrasound transmission and it performs both ultrasound and optoacoustic data acquisitions on a multi-channel board. In order to enhance operation of the memory of the FPGA, an external memory buffer can be used. In an embodiment, the FPGA allows rapid reprogramming of ultrasonic data acquisition with signal/frame repetition rate of about 2 to 20 kHz to optoacoustic data acquisition with signal/frame repetition rate of about 10-20 Hz, and also configures the structure of gates and internal memory structure and size to allow

real-time switching between ultrasound emission and detection, laser synchronization, and system controls. In an embodiment, multiple FPGAs can be used to enhance the system performance. In an embodiment, in the ultrasound and optoacoustic modes, the FPGA clock can be changed by the appropriate time-division multiplexing (TDM). In an embodiment, the design of a multi-channel electronic data acquisition system can be based on modules, with a module typically being from 16 to 128 channels, although 256 channels or more may be appropriate in some applications. In an embodiment, the design of a multi-channel electronic data acquisition system has 64 channels.

In order to achieve dual modality operation of the optoacoustic/ultrasonic system, a separate optoacoustic electronic system could also be combined with a separate ultrasonic electronic system through a single probe. In an embodiment, the probe has a cable that has a Y-split to connect the probe to optoacoustic and ultrasonic electronic systems. In an embodiment, a programmable electronic switch allows one to send the detected signal from the probe (transducer array) either to the optoacoustic electronics (to operate in optoacoustic mode) or to the ultrasonic electronics and from the ultrasonic electronics to the probe (to operate in ultrasound mode). In an embodiment, a synchronization trigger signal is sent to the optoacoustic and ultrasonic systems sequentially, so that the optoacoustic and ultrasonic images are acquired one after the other.

Processing, Reconstruction and Display of Images Signal Processing

In various embodiments, a goal of the diagnostic imaging procedure is to display each pixel with a brightness that correctly replicates the originally generated signals in each voxel of tissue displayed on the image. On the other hand, intrinsic pressure signals generated by optical pulses within tissues may be significantly altered in the course of propagation through tissue and especially in the course of detection and recording by the ultrasonic transducers and the electronics subsystem.

In an embodiment, detected signals are processed to reverse alterations and restore original signals. In an embodiment, such reversal can be achieved through deconvolution of the impulse response (IR) of the system. In an embodiment, the impulse response can be measured by recording and digitizing a delta-function ultrasonic signal generated by short (nanosecond) laser pulses in a strongly absorbing optical medium with high thermoelastic expansion coefficient.

One component of the impulse response is the acousto-electrical impulse response, which provides for the optoacoustic or ultrasonic signal distortions due to the properties of the ultrasonic transducers, cables and analog electronics. A second part of the impulse response is the spatial impulse response that provides for the signal distortions associated with finite dimensions of the ultrasonic transducers. In various embodiments, large transducers can integrate ultrasonic waves incident at an angle, whereas point-source-like transducers can provide perfect or near perfect delta-function spatial impulse response.

In an embodiment, any distortions in acousto-electrical impulse response can be reversed by the impulse response deconvolution from the detected signals. However, possible distortions in the spatial impulse response can be avoided by designing transducers with small dimensions within the image plane. In an embodiment, the dimensions of the transducers are much smaller than the shortest wavelength of the ultrasound that may be detected or emitted by the transducers.

FIGS. 10A-10C show examples of the impulse response of an ultrasonic transducer with a relatively narrow band of sensitivity **1010**, the impulse response of an ultrawide-band ultrasonic transducer **1020** and ultrasonic spectra of the transducer sensitivity as a function of frequency for ultrawide-band and narrow band resonant transducers **1030**.

In an embodiment, the first step in processing an optoacoustic signal in an imaging system that produces two-dimensional optoacoustic images is deconvolution of the acousto-electrical impulse response.

FIGS. 11A and 11B provide an illustrative example of the deconvolution of impulse response of transducers from the detected optoacoustic signals **1110**, where deconvolution restores the original, unaltered, N-shaped pressure signals **1120**.

In an embodiment, the second step in processing an optoacoustic signal is signal filtering to remove noise using a signal filter. In an embodiment, the signal filter is based on a wavelet transform that operates simultaneously in the frequency and time domain. In an embodiment, such a wavelet filter is capable of filtering certain frequency components of the signal that belong to noise and appear at a given time, while preserving similar frequency components of the useful signal that appear at a different time. In an embodiment, the frequency spectrum of a wavelet filter replicates the frequency band of a typical N-shaped optoacoustic signal while simultaneously providing smooth window edges which do not cause signal distortions upon convolution.

In an embodiment, such a wavelet filter is useful in optoacoustic imaging in its capability to restore the original pressure profile generated in tissue prior to pressure propagation. In the course of propagation through tissue, the originally positive pressure signal converts into a bipolar (compression/tension) profile. Therefore, reconstruction of an image of absorbed optical energy (optoacoustic image) requires a transformation that starts with bipolar signals and provides for all-positive values of the optoacoustic image intensities. In an embodiment, a multi-scale wavelet filter, for example, a filter that simultaneously integrates the signal over time and provides summation of a number of frequency bands present in the signal, can convert bipolar pressure signals into monopolar signal representing thermal energy or originally generated positive pressure.

FIGS. 12A-12C provide an illustrative example of wavelet filtered N-shaped optoacoustic signals restored to their original rectangular pressure profile by summation of all scales corresponding to frequency ranges from low to high for five scales **1210**, seven scales **1220** and nine scales **1230**.

In various embodiments, wavelet filtering permits enhancements of objects on the image within certain range of dimensions. An imaging operator (ultrasonic technician or diagnostic radiologist) typically desires to better visualize a tumor with specific dimensions and other objects, such as blood vessels, with their specific dimensions. In an embodiment, the wavelet filter allows the operator to apply specific selection of scales of the wavelet filter than would enhance only objects of certain sizes and suppress object of other unimportant sizes. In an embodiment, boundaries can be well visualized for objects of any size, so the high-frequency wavelet scales are beneficial for the image quality and are included in the selection of scales. In an embodiment, for a mathematically correct tomographic reconstruction, a ramp filter can be applied to the signal, which can linearly enhance contribution of higher frequencies.

Image Reconstruction

In various embodiments, image reconstruction typically uses radial back-projection of processed and filtered signals onto the image plane. However, due to the limited field of view available from small hand-held probes, only an incomplete data set can be obtained. As a result, the 2D optoacoustic images may include artifacts distorting the shape and brightness of the objects displayed on the images. In an embodiment, aperture integrated normalized radial back projection is used to correct some of the reconstruction artifacts that are observed in limited aperture optoacoustic tomography.

FIG. 13 provides an illustrative diagram of radial back-projection where each transducer element aperture is weighted and normalized for the total aperture of the transducer array.

In an embodiment, $T_k, -T_{k+4}$, **1311-1315**, are the transducers **1310** in the array, $B_{i,j}$ is the brightness (intensity) of a pixel with coordinates (i,j) , $\omega_{i,j,k}$ **1320, 1330** is the angular portion of optoacoustic wave front emitted by the pixel (i,j) as it is visualized by the transducer $\#k$, $\Omega_{i,j} = \sum \omega_{i,j,k}$ (sum of all $\omega_{i,j,k}$) is the portion of the optoacoustic wave front emitted by pixel (i,j) as it is visualized by the entire transducer array, and $S_{i,j,k}$ is the sample of the optoacoustic signal measured by k^{th} transducer and used in reconstruction of the brightness of the pixel (i,j) . Various backpropagation algorithms can be used to normalize an optoacoustic image.

In an embodiment, a backpropagation algorithm can be expressed as:

$$B_{i,j} = \sum_k S_{i,j,k} \quad (1)$$

However, in at least some embodiments, aperture normalized backprojection produces superior image results. In an embodiment, the aperture normalized backprojection can be expressed as:

$$B_{i,j} = \frac{1}{\Omega_{i,j}} \sum_k S_{i,j,k} \Omega_{i,j,k} \quad (2)$$

FIGS. 14A and 14B provide an illustrative example of optoacoustic tomographic images **1410** and **1420** of an imaging slice through a tumor angiogenesis model. In the first image **1410**, a backpropagation algorithm, such as the first algorithm immediately above, is used to normalize the image. The resulting image has strong, bright arc-shaped artifacts **1412** around the blood vessels **1414** that are close to array surface. In the second image **1420**, aperture normalized backprojection algorithm, such as the second algorithm immediately above, is used to normalize the image. As can be seen, the aperture normalized backprojection algorithm corrects image brightness and reduces the arc-shaped artifacts.

FIGS. 15A and 15B provide an illustrative example of optoacoustic tomographic images **1510** and **1520** of a point spread function as visualized with flat linear probe using **1510** a backpropagation algorithm, such as the first algorithm immediately above, and **1520** an aperture normalized backprojection algorithm, such as the second algorithm immediately above. As can be seen, the aperture normalized backprojection algorithm corrects image brightness and reduces artifacts.

Image Processing and Display

In an embodiment, the optoacoustic image palette is equalized to diminish effects of light distribution within

tissue. Such equalization transforms the dynamic range of optoacoustic images for better visualization of both shallow and deep objects.

FIGS. 16A and 16B provide an illustrative example of optoacoustic images 1610 and 1620 of a phantom with hairs embedded at different depths where the first image 1610 was created using a an embodiment of a standard palette and the second image 1620 was created using an embodiment of a depth-normalized palette. As can be seen, utilizing the depth-normalized palette enhances visibility of deep objects in the illustrated embodiment.

In an embodiment, principal component analysis (PCA) on a single optoacoustic image acquisition (different channels) is used to remove cross-correlated signal noise. Principal component analysis on a dataset of optoacoustic signals can remove correlated image clutter. Principal component analysis on optoacoustic frames can also remove correlated image clutter.

FIGS. 17A and 17B provide an illustrative example of optoacoustic images 1710 and 1720 of a phantom of a spherical simulated tumor obtained with flat linear probe. The first image 1710 is a raw image that was not subjected to principal component analysis processing. The second image 1720 has been subjected to principal component analysis processing with first principal component deconvolution. As can be seen, utilizing principal component analysis processing enhances image quality by, inter alia, reducing artifacts.

In an embodiment, design features of signal and image processing of the present disclosure can be summarized in the Table 2 as follows:

TABLE 2

Summary of signal and image processing.	
System Feature	Advantages
Operator-assisted boundary tracking on ultrasonic and optoacoustic images	Can improve quantitative optoacoustic diagnostics by evaluating the diagnostic parameters within the tumor boundary defined on US images Diagnostics can be enhanced by morphological analysis of the tumor boundary
Aperture integrated normalized radial back projection	Corrects some of the reconstruction artifacts that are observed in a limited aperture optoacoustic tomography
Equalization of the optoacoustic image palette to diminish effects of light distribution within the tissue	Transforms dynamic range of optoacoustic images for better visualization of both shallow and deep objects
Principal component analysis (PCA) of the optoacoustic signal data	PCA on a single optoacoustic acquisition (different channels) is a fast and efficient way to remove cross-correlated signal noise PCA on a dataset of optoacoustic signals removes correlated image clutter PCA on optoacoustic frames removes correlated image clutter
Optoacoustic imaging system with quantitative assessment of total hemoglobin, blood oxygenation, and water	Cancer diagnostics based on those parameters or a single malignancy index (tHb*water/oxygenation) with respect to average background
Wavelet transform that enhances images of objects within certain dimension range	Operator can easily select the maximum size of the objects to be enhanced on the image. Everything larger will be filtered out
Adaptive beam-forming for optoacoustic imaging	Allows individual reconstruction on a family of radial wavelet sub-bands

Diagnostic Image Reprocessing

The principles of functional diagnostic imaging can be based on the tumor pathophysiology. For example, malignant tumors have enhanced concentration of the total hemoglobin and reduced level of oxygen saturation in the hemoglobin of blood. In an embodiment, optoacoustic images can be reprocessed and converted into, inter alia, images of (i) the total hemoglobin [tHb] and (ii) the oxygen saturation of hemoglobin [SO₂]. FIG. 18 demonstrates an example of two breast tumors

FIG. 18 shows a diagram illustrating tumor differentiation based on absorption coefficients at two wavelengths, 755 nm, 1810, and 1064 nm, 1820, which match the local maximum (757 nm) and minimum (1064 nm) of the ratio of absorption by hemoglobin (hypoxic blood) to absorption by oxyhemoglobin. As can be seen, a malignant tumor, 1830, has a higher absorption coefficient at 757 nm than a benign tumor, 1840, whereas the benign tumor, 1840, has a higher absorption coefficient at 1064 nm than a malignant tumor, 1830.

FIG. 19 illustrates tumor differentiation by optoacoustic imaging based on absorption coefficients at two wavelengths 1910 and 1920 in a phantom. At 757 nm, 1920, a model of a malignant tumor is clearly visible, 1922, whereas the model of the malignant tumor, 1922, is not visible at 1064 nm, 1910.

FIG. 20A shows an optoacoustic image of two intersecting tubes filled with blood having different levels of blood [SO₂] (98% in the left tube, and 31% in the right tube). The tubes were placed in 1% fat milk with optical properties similar to those found in the human breast. The wavelength

of laser illumination used for this image is 1064 nm. FIG. 20B shows a photograph of an experimental setup that includes artificial blood vessels placed in milk solution and imaged using arc-shaped optoacoustic probe. FIG. 20C shows coregistered 2D cross-sectional anatomical and functional images of blood vessel tubes showing six image panels: (1—upper left) ultrasound image depicting anatomy of the body with vessels; (2—upper right) optoacoustic image obtained at the wavelength of 757 nm; (3—lower right) optoacoustic image obtained at the wavelength of 1064 nm; (4—lower left) functional image of the total hemoglobin [tHb]; (5—lower center) functional image of the blood oxygen saturation [SO₂]; (6—upper center) functional image of the blood oxygen saturation presented only in the area of maximum concentration of the total hemoglobin. Raw optoacoustic images depicted in FIG. 20C in the upper right and lower right panels demonstrate different brightness of blood vessels having blood with different level of the total hemoglobin concentration [tHb] and blood oxygen saturation [SO₂], accurate quantitative measurements could be performed under conditions of normalized fluence of the optical illumination of tissue in the body as a function of depth. These optoacoustic images were used to reconstruct functional images of the total hemoglobin [tHb] and the blood oxygenation [SO₂]. All functional images displayed in FIG. 20C are coregistered and superimposed with the anatomical image of tissue structure for better correlation of features.

FIGS. 21A and 21B show optoacoustic signal amplitude as a function of blood oxygen saturation (with constant hematocrit) under laser illumination at the wavelength of 1064 nm in FIG. 21A and at 757 nm in FIG. 21B. These plots illustrate that blood oxygen saturation can be monitored with optoacoustic imaging. Specifically, this embodiment illustrates quantitative data based on measurements of the optoacoustic signal amplitude in blood having various levels of oxygen saturation (from 30% to 98%) and hematocrit of 38 g/dL of hemoglobin [tHb] in erythrocytes. As predicted by the published absorption spectra of blood, the optoacoustic signal amplitude at 1064 nm illumination increases with increased level of oxygen saturation, while the optoacoustic signal amplitude decreases with increased blood oxygenation at 757 nm illumination wavelength.

FIG. 22 illustrates optical absorption spectra of the main tissue chromophores absorbing optical energy in the near-infrared range: hemoglobin, oxyhemoglobin and water. Preferred laser wavelengths for functional imaging are 757 nm and 1064 nm matching max and min ratio of [HHb]/[O₂Hb], while the wavelength of 800 nm is the best for calibration purposes through measurements of the total hemoglobin [tHb].

FIGS. 23A and 23B illustrate coregistered functional and anatomical imaging of breast tumors in phantoms accurately replicating optical and acoustic properties of an average breast with tumors. FIG. 23A shows 2D images of: model of malignant tumor morphology based on ultrasound (left), the same anatomical image coregistered with functional image of the total hemoglobin concentration (center) and with functional image of the blood oxygenation (right). FIG. 23B shows 2D images of a model benign tumor: morphology image based on ultrasound (left), the same anatomical image coregistered with functional image of the total hemoglobin concentration (center) and with functional image of the blood oxygenation (right).

FIGS. 24A and 24B illustrate coregistered functional and anatomical imaging of breast tumors. FIG. 24A shows 2D images of invasive ductal carcinoma, a malignant tumor

with rough boundaries, heterogeneous morphology, high concentration of total hemoglobin and low oxygen saturation (hypoxia). The malignant tumor morphology is based on ultrasound in the left image, and the same anatomical image coregistered with functional image of the blood oxygenation in the center image and with functional image of the total hemoglobin concentration in the right image. FIG. 24B shows 2D images of a breast with Fibroadenoma, a benign tumor with relatively round boundaries, normal concentration of oxyhemoglobin and relatively low total hemoglobin. Breast morphology is based on ultrasound in the left image, and the same anatomical image is coregistered with a functional image of the blood oxygenation in the center image and with a functional image of the total hemoglobin concentration in the right image.

CONCLUSION

While some embodiments can be implemented in fully functioning computers and computer systems, various embodiments are capable of being distributed as a computing product in a variety of forms and are capable of being applied regardless of the particular type of machine or computer-readable media used to actually effect the distribution.

At least some aspects disclosed can be embodied, at least in part, in software. That is, the techniques described herein may be carried out in a special purpose or general purpose computer system or other data processing system in response to its processor, such as a microprocessor, executing sequences of instructions contained in a memory, such as ROM, volatile RAM, non-volatile memory, cache or a remote storage device.

Routines executed to implement the embodiments may be implemented as part of an operating system, firmware, ROM, middleware, service delivery platform, SDK (Software Development Kit) component, web services, or other specific application, component, program, object, module or sequence of instructions referred to as "computer programs." Invocation interfaces to these routines can be exposed to a software development community as an API (Application Programming Interface). The computer programs typically comprise one or more instructions set at various times in various memory and storage devices in a computer, and that, when read and executed by one or more processors in a computer, cause the computer to perform operations necessary to execute elements involving the various aspects.

A machine-readable medium can be used to store software and data which when executed by a data processing system causes the system to perform various methods. The executable software and data may be stored in various places including for example ROM, volatile RAM, non-volatile memory and/or cache. Portions of this software and/or data may be stored in any one of these storage devices. Further, the data and instructions can be obtained from centralized servers or peer-to-peer networks. Different portions of the data and instructions can be obtained from different centralized servers and/or peer-to-peer networks at different times and in different communication sessions or in a same communication session. The data and instructions can be obtained in entirety prior to the execution of the applications. Alternatively, portions of the data and instructions can be obtained dynamically, just in time, when needed for execution. Thus, it is not required that the data and instructions be on a machine-readable medium in entirety at a particular instance of time.

Examples of computer-readable media include but are not limited to recordable and non-recordable type media such as volatile and non-volatile memory devices, read only memory (ROM), random access memory (RAM), flash memory devices, floppy and other removable disks, magnetic disk storage media, optical storage media (e.g., Compact Disk Read-Only Memory (CD ROMS), Digital Versatile Disks (DVDs), etc.), among others.

In general, a machine readable medium includes any mechanism that provides (e.g., stores) information in a form accessible by a machine (e.g., a computer, network device, personal digital assistant, manufacturing tool, any device with a set of one or more processors, etc.).

In various embodiments, hardwired circuitry may be used in combination with software instructions to implement the techniques. Thus, the techniques are neither limited to any specific combination of hardware circuitry and software nor to any particular source for the instructions executed by the data processing system.

Although some of the drawings illustrate a number of operations in a particular order, operations that are not order dependent may be reordered and other operations may be combined or broken out. While some reordering or other groupings are specifically mentioned, others will be apparent to those of ordinary skill in the art and so do not present an exhaustive list of alternatives. Moreover, it should be recognized that the stages could be implemented in hardware, firmware, software or any combination thereof.

In the foregoing specification, the disclosure has been described with reference to specific exemplary embodiments thereof. It will be evident that various modifications may be made thereto without departing from the broader spirit and scope as set forth in the following claims. The specification and drawings are, accordingly, to be regarded in an illustrative sense rather than a restrictive sense.

The invention claimed is:

1. A method for imaging tissue of at least a portion of a body, comprising:

- a) delivering ultrasonic pulses into the tissue and detecting backscattered ultrasonic signals reflected from structural tissue boundaries associated with body morphology;
- b) sequentially delivering to the tissue at least two optical pulses having different spectral bands of electromagnetic energy and detecting transient ultrasonic signals resulting from selective absorption of each of the at least two optical pulses in hemoglobin and oxyhemoglobin of blood contained in tissues;
- c) processing detected ultrasonic signals to remove noise, to revert signal alterations in the course of signal propagation through tissue and through the detection system components, and to restore a temporal shape and ultrasonic spectrum of the detected ultrasonic signals, and further processing signals with a family of wavelets to generate individual subbands;
- d) performing image reconstruction and further processing to generate morphological images of tissue structures coregistered and superimposed with partially transparent functional images reflecting total hemoglobin concentration and blood oxygen saturation, wherein image reconstruction and further processing comprises performing an adaptive beam-forming on each of the individual subbands, the adaptive beam-forming permitting reconstruction from individual adaptive reconstructions; and,

e) repeating steps a) through d) at a video frame rate such that real-time images display tissue functional and morphological changes as they occur.

2. The method of claim 1, in which three or more optical pulses each having different spectral bands of electromagnetic radiation are sequentially delivered to the tissue so as to generate functional images with improved accuracy that reflect significant molecular chromophores of tissue.

3. The method of claim 2, in which the molecular chromophores of tissue comprise water.

4. The method of claim 2, in which the molecular chromophores of tissue comprise lipids.

5. The method of claim 2, in which four optical pulses each having different spectral bands of electromagnetic radiation are sequentially delivered to the tissue.

6. The method of claim 1, in which spectral bands of the two optical pulses are selected so that one of them matches local maximum peak of hemoglobin absorption around 757 nm and the other matches the spectral range around 1064 nm corresponding to the maximum ratio in the optical absorption of oxyhemoglobin to that of hemoglobin.

7. The method of claim 1, further comprising a step of indicating tumor differentiation based at least in part on absorption coefficients measured in the tumor at first and second wavelengths.

8. The method of claim 7, wherein the first wavelength comprises 757 nanometers.

9. The method of claim 7, wherein the second wavelength comprises 1064 nanometers.

10. The method of claim 7, wherein the step of tumor differentiation comprises displaying either:

- a. a relatively smooth shape of a tumor, or tissue surrounding a tumor, superimposed with relatively low elevation in concentration of the total hemoglobin and normal blood oxygen saturation to indicate a benign tumor, or
- b. displaying a rough shape of a tumor, or tissue surrounding the tumor, superimposed with high elevation in the total hemoglobin and low blood oxygen saturation to indicate a malignant tumor.

11. The method of claim 1, further comprising a step of renormalizing an image display palette by reducing relative brightness of image pixels corresponding to the tissue's surface, thereby amplifying relative brightness of pixels corresponding to larger depths in tissue, so as to make objects located at larger depths visible with greater contrast.

12. The method of claim 1, further comprising a step of using optoacoustic and ultrasonic contrast agents to enhance visualization of tissue morphology and contrast of functional information within a portion of the body being imaged.

13. The method of claim 1, further comprising a step of using optoacoustic and ultrasonic contrast agents to enhance characterization of distribution of predetermined types of molecules, cells or tissues in the body.

14. The method of claim 1, wherein the step of performing image reconstruction and further processing comprises:

- a. processing signals into individual families of radial wavelet subbands; and
- b. performing adaptive beamforming on each of the individual families of radial wavelet subbands, the adaptive beam-forming permitting individual adaptive reconstructions.

15. The method of claim 1, wherein the family of wavelets is a family of radial wavelets.

专利名称(译)	双模态光声成像的方法		
公开(公告)号	US9757092	公开(公告)日	2017-09-12
申请号	US13/667830	申请日	2012-11-02
[标]申请(专利权)人(译)	SENO医疗INSTR		
申请(专利权)人(译)	SENO医疗仪器公司.		
当前申请(专利权)人(译)	SENO医疗器械, INC.		
[标]发明人	ORAEVSKY ALEXANDER A ERMILOV SERGEY A CONJUSTEAU ANDRE BRECHT PETER NADVORETSKIY VYACHESLAV SU RICHARD HERZOG DONALD G CLINGMAN BRYAN ZALEV JASON		
发明人	ORAEVSKY, ALEXANDER A. ERMILOV, SERGEY A. CONJUSTEAU, ANDRE BRECHT, PETER NADVORETSKIY, VYACHESLAV SU, RICHARD HERZOG, DONALD G. CLINGMAN, BRYAN ZALEV, JASON		
IPC分类号	G06K9/00 A61B8/08 A61B5/00 A61B8/00		
CPC分类号	A61B8/5215 A61B5/0035 A61B5/0095 A61B8/4416 A61B8/48 A61B8/5207 A61B8/5261 A61B8/4477 A61B8/4494 A61B8/481		
审查员(译)	MOYER, ANDREW		
其他公开文献	US20130301380A1		
外部链接	Espacenet USPTO		

摘要(译)

一种实时成像方法, 通过应用相同的手持式探头生成和检测超声波和光声信号, 提供超声成像和光声成像。这些信号被数字化, 处理并用于重建与血液血红蛋白指数和血氧指数的两个功能参数的图叠加的解剖图。血液血红蛋白指数表示相对于背景血液浓度的诊断感兴趣区域中的血液血红蛋白浓度变化。血氧指数表示相对于血氧合的背景水平的诊断感兴趣区域中的血氧变化。这些核心配准图可用于非侵入性地区分恶性肿瘤与良性肿块和囊肿。

1120

